Available online at www.sciencedirect.com

SCIENCE DIRECT®

Sedimentary Geology 178 (2005) 285–313

Sedimentary Geology

www.elsevier.com/locate/sedgeo

Grains in motion: A review

J.P. Le Roux

Departamento de Geología, Facultad de Ciencias Físicas y Matemáticas, Universidad de Chile, Casilla 13518, Correo 21, Santiago, Chile

Received 29 June 2004; received in revised form 17 May 2005; accepted 20 May 2005

Abstract

This review paper aims to present a practical, integrated procedure for the prediction of sediment transport rates in both the continental and marine environment, based on the settling velocity of particles. Such studies have important applications in diverse fields such as civil and coastal engineering, sedimentology and environmental geology, where they can assist in flood control and the prevention of contaminant dispersal by wind and water, as well as the siltation of dams and harbours. The formation of placer deposits including gold, diamonds and other heavy minerals is also controlled by sediment transport processes, so that these studies can form the basis for more efficient exploration programs.

The first part of the paper discusses some basic principles important in sediment transport, followed by an overview of published methods to determine the settling velocity of differently shaped particles, including natural grains. The application of settling velocity to predict the entrainment threshold of sediments on plane, horizontal and inclined beds by unidirectional currents and oscillatory waves is then discussed, which finally leads to the determination of sediment transport rates over plane and rippled beds. The validity of this approach to natural conditions is tested against published field data where possible. Other, widely used methods are also critically discussed, pointing out severe problems in current sampling technology and the calculation of bedload transport in natural environments.

© 2005 Elsevier B.V. All rights reserved.

Keywords: Particle shape; Settling velocity; Sediment transport; Bedload; Suspended load

1. Introduction

The behaviour of natural sediment grains in water and air, with applications in civil and coastal engineering, sedimentology, environmental and economic geology (e.g., Le Roux, 1990, 1991a, 1993; Le Roux and Brynard, 1994) has been studied over the past two centuries, with incremental advances continually expanding our understanding of this subject. Solid–fluid interactions can be extremely complex, so that the most logical way to approach the matter is by starting with relatively simple, straightforward processes such as the behaviour of single spheres settling in quiet fluids. These studies can form a basis for more advanced research on sediment transport and the modelling of depositional systems.

E-mail address: jroux@ing.uchile.cl.

0037-0738/$ - see front matter © 2005 Elsevier B.V. All rights reserved.
doi:10.1016/j.sedgeo.2005.05.009

Because the literature on sediment transport is vast, this paper focuses on one particular approach to the problem by building on a platform of grain settling velocity. Having an empirical rather than theoretical emphasis, it endeavours to be practical in that no difficult-to-obtain variables or field measurements are required. For the sake of completeness, an overview of some basic principles of sediment transport is included.

2. Dimensions, dimensionless numbers and dimensional analysis

The properties of most substances can be expressed in terms of three primary dimensions, namely mass (M), length (L) and time (T). For example: fluid density $\rho = M\,L^{-3}$; dynamic viscosity $\mu = M\,L^{-1}T^{-1}$; velocity $U = L\,T^{-1}$; acceleration of gravity $g = L\,T^{-2} = 981$ cm s^{-1}. With reference to their dynamic behaviour in fluids, solid particles can therefore be described in terms of their diameter ($D = L$), density (ρ_s) and shape, the latter being expressed, for example, by different relationships of the long, intermediate and short orthogonal axes (D_l, D_i, D_m). The most important properties of fluids include their density (ρ), dynamic or kinematic viscosity (μ, υ), mean flow velocity (U_m) and flow depth (d).

Dimensionless numbers are groups of variables arranged in such a way that their primary dimensions cancel each other out. A well-known example of such a dimensionless group is the Reynolds number $Re = \rho LU/\mu$, which in primary dimensions can be written as $(M\,L^{-3})(L)(L\,T^{-1})/M\,L^{-1}T^{-1} = 1$.

Dimensional analysis is a method to arrange different variables in dimensionless groups, with the latter representing "variables" by themselves (Buckingham, 1914, 1921). This has the advantage of greatly reducing the number of variables that normally have to be considered separately in a series of experiments. For example, a dimensionless sphere diameter D_{ds} (Dietrich, 1982) is used throughout this paper, which is given by

$$D_{ds} = D_s \sqrt[3]{\left(\rho g \rho_\gamma / \mu^2\right)} \tag{1}$$

where D_s is the sphere diameter and ρ_γ is the submerged particle density, i.e. $\rho_s - \rho$. The same variables play a role in the settling velocity of the sphere and can be rearranged to get a dimensionless sphere settling velocity W_{ds}.

$$W_{ds} = W_s \sqrt[3]{\left(\rho^2 / \mu g \rho_\gamma\right)} \tag{2}$$

where W_s is the sphere settling velocity.

Plotting W_{ds} against D_{ds} allows the settling velocity of spheres of different sizes and densities in fluids of different densities and viscosities to be calculated.

The methodology of dimensional analysis can be explained best by using an example: Consider the drag force of a fluid (F_D) on a quartz grain, which depends on D, U, ρ and μ. Therefore, $F_D = f(D, U, \rho, \mu)$. If these variables could be combined into a dimensionless drag force, the number of variables and therefore the required number of experiments would be reduced drastically. Using Buckingham's Pi-theorem, the following steps are required:

- Make a list of all variables that could play a role in the experiments. In this case: $G(F_D, D, U, \rho, \mu)$.
- Determine the number (m) of primary dimensions (M, L, T) involved. The n variables can be arranged into $n - m$ independent dimensionless groups ($m = 3$, $n - m = 2$).
- Express all variables (es) in terms of their primary dimensions: $F_D = ML\,T^{-2}$; $D = L$; $U = L\,T^{-1}$; $\rho = M\,L^{-3}$; $\mu = M\,L^{-1}T^{-1}$.
- Choose m variables from n (the so-called primary or repeating es) so that they contain each primary dimension at least once.
- Form dimensionless groups with the primary es and each of the other es. This is accomplished by expressing the es in terms of exponents. The dimensionless groups are called π-terms: e.g. $\pi_1 = F_D D^a U^b \rho^c$; $\pi_2 = \mu D^d U^e \rho$. Because a dimensionless drag force is required, F_D should not be raised to a power. To get $\pi_1$dimensionless, determine the values of a, b and c so that their product is 1. Write each π_1-term in terms of its primary dimensions and solve for a, b and c.

$$\pi_1 = \left(MLT^{-2}\right)(L)^a\left(LT^{-1}\right)^b\left(ML^{-3}\right)^c = M^0L^0T^0$$

$$M = 1 + c = 0, \text{ therefore } c = -1$$

$$T = -2 - b = 0, \text{ therefore } b = -2$$

$$L = 1 + a + b - 3c = 4 + a + b = 0,$$
therefore $a = -2$

$$\pi_1 = F_D D^{-2} U^{-2} \rho^{-1} \text{ or } F_D / D^2 U^2 \rho = 1$$

π_1 is a dimensionless drag coefficient C_d. In the same way, π_2 is found to be $\mu\rho^{-1}D^{-1}U^{-1} = \mu/\rho DU = 1/Re = 1$.

Originally, there were 5 variables (F_D, D, U, ρ, μ), but now there are only two (π_1, π_2), which can be plotted on a normal, 2D graph. The curve can be obtained by changing only one of the variables (e.g. U).

If an important variable is left out accidentally (e.g. g), the cross-plots would form a scattered band. If, on the other hand, an irrelevant variable is included, the cross-plots would define a line parallel to the axis of the dimensionless group containing the variable.

3. The nature of solids and fluids

3.1. Properties of solids

A solid obeys Hooke's law in that strain is proportional to stress; i.e. the solid deforms under stress but recovers its original shape when the stress is relieved. If the stress exceeds the elastic limit, however, the material deforms or fractures permanently. Solids typically have high shear and compressive strengths. The dynamic behaviour of solid grains in fluids is a function of their size, shape and density. While the density is easily determined, the first two properties are far more complex than is generally appreciated (Pettijohn, 1975; Winkelmolen, 1982; Illenberger, 1991).

3.1.1. Particle size

Particle size can be expressed as mass (M), volume (V), surface or cross-sectional area (A), diameters of different intersections or projections (D_x), as well as the settling velocity (W). For individual grains, three orthogonal axes are commonly measured, based on the maximum projection area of the grain (Krumbein, 1941). The longest diameter perpendicular to this surface is the short axis D_m, the short side of a tangential rectangle to the projection is the intermediate axis D_i, and the long side of the rectangle is the long axis D_l (Fig. 1). Other methods are based on the

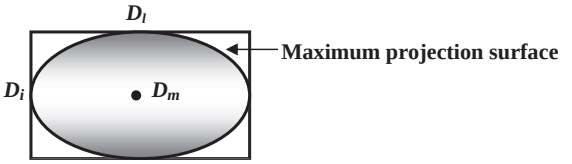

Fig. 1. Triaxial dimensions of ellipsoidal particle.

premise that the particle is a sphere or that its size can be expressed as the diameter of an equivalent sphere (which has the same volume as the grain). The last expression of size is known as the nominal diameter (D_n), which is given by (Wadell, 1932, 1933)

$$D_n = \sqrt[3]{(6V/\pi)} = \sqrt[3]{(D_l D_i D_m)}. \quad (3)$$

For natural sediment samples, these measures are impractical and traditionally two methods have been used to determine the grain size distribution, viz. sieve analysis and settling analysis. The size as determined by sieve analysis is expressed as the sieve diameter (D_v), which is construed as the size of the largest sphere that would pass through the retaining sieve mesh. However, the actual dimensions depend largely on the grain shapes and the results are influenced by screen imperfections and differences in sieving procedures. To convert the retaining sieve size into the nominal diameter of its equivalent sphere, it is multiplied by 1.32 (Komar and Cui, 1984).

The size as determined by settling analysis, on the other hand, is expressed in terms of the equivalent sedimentation or fall diameter (D_w), which is the diameter of a sphere with the same settling velocity. Similar constraints apply in this case, as the settling velocity is largely dependent on the grain shape. The advantage of using D_w is that it is a behavioural measure controlled partly by the same variables involved in sediment entrainment, so that it is preferable to D_v (Willetts et al., 1982; Kench and McLean, 1997). However, as many sediment transport studies have been based on D_v data, it is still convenient to use this expression of size.

The relationship between the grain size of natural particles as obtained from sieve analysis (D_v) and that derived from settling tube analysis (D_w) was investigated by Le Roux and Brodalka (2004). Using the data sets of Cheng (1997), they plotted the observed dimensionless settling velocities W_{dw} against the cal-

culated dimensionless settling velocities of equivalent sieve diameter grains (W_{dvn}). As the distribution is complex, four different curves were fitted to the data. These are given by

$$W_{dvn} = 1.3098 W_{dw}^{0.9897} \text{ for } W_{dw}<0.7509 \quad (4)$$

$$W_{dvn} = 0.0753 W_{dw}^2 + 0.8529 W_{dw} + 0.3036 \text{ for } 0.7509<W_{dw}<8.936 \quad (5)$$

$$W_{dvn} = 0.5486 W_{dw}^2 - 7.4271 W_{dw} + 36.5 \text{ for } 8.936<W_{dw}<10.3956 \quad (6)$$

$$W_{dvn} = -0.0289 W_{dw}^2 + 2.1646 W_{dw} - 0.8018 \text{ for } 10.3956<W_{dw}<17.4857. \quad (7)$$

The grain fall diameter D_w as obtained from the settling tube analysis is first converted to its dimensionless form D_{dw} using Eq. (1), after which one of Eqs. (29)–(33) is employed (substituting D_{dw} for D_{ds}) to obtain W_{dw} from D_{dw}. W_{dvn} is then calculated from W_{dw} using Eqs. (4)–(7). Subsequently, the appropriate one of Eqs. (34)–(38) is used (substituting W_{dvn} for W_{ds}) to determine D_{dv} from W_{dvn}. D_{dv} is then converted to D_v by Eq. (1). This procedure ensures that the influence of shape on the settling velocity is taken into account, as Eqs. (4)–(7) are linked to the Hofmann (1994) shape index of natural grains (Le Roux, 2002b).

3.1.2. Particle shape

Particle shape is an even more complex subject than size. Different shape indices have therefore been proposed, including the flatness index (Wentworth, 1922), the oblate–prolate index (Dobkins and Folk, 1970), the disk-rod index and rod index (Illenberger, 1991), as well as several measures of sphericity (Wadell, 1932; Rubey, 1933; Krumbein, 1941; Corey, 1949; McNown and Malaika, 1950; Aschenbrenner, 1956; Janke, 1966; Hofmann, 1994). Many of these shape indices have proved useful to determine the settling velocity of non-spherical particles (Komar and Reimers, 1978; Baba and Komar, 1981a,b). Le Roux (1996, 1997a) demonstrated that the Hofmann (1994) shape entropy H_r gives the best results for ellipsoidal grains. This shape factor is given by

$$H_r = -[(p_l \ln p_l) + (p_i \ln p_i) + (p_m \ln p_m)]/1.0986 \quad (8)$$

where p_l, p_i and p_m are the proportions of the long, intermediate and short axes of the grain. For example, the proportion of D_i is expressed as

$$p_i = D_i/(D_l + D_i + D_m). \quad (9)$$

Le Roux (2004b) subsequently proposed a new shape factor DES, the deviation from the equivalent sphere, given by

$$\text{DES} = 1 - (D_a/D_b) \quad (10)$$

where a/b represents any of the 6 possible orthogonal axial ratios of a grain with the same volume as its equivalent sphere.

3.2. Properties of fluids

3.2.1. Fluid density and viscosity

The density and viscosity of any particular fluid depends on its temperature (°C). The density of fresh water is given (accurate to the 4th decimal) by

$$\rho = -5 \times 10^{-10} {}^\circ\text{C}^4 + 8 \times 10^{-8} {}^\circ\text{C}^3 - 9 \times 10^{-6} {}^\circ\text{C}^2 + 7 \times 10^{-5} {}^\circ\text{C} + 0.99985 \text{ for } 0<{}^\circ\text{C}<26 \quad (11)$$

$$\rho = -5 \times 10^{-10} {}^\circ\text{C}^4 + 8 \times 10^{-8} {}^\circ\text{C}^3 - 9 \times 10^{-6} {}^\circ\text{C}^2 + 7 \times 10^{-5} {}^\circ\text{C} + 0.99995 \text{ for } 26<{}^\circ\text{C}<40. \quad (12)$$

The dynamic viscosity μ of water (also accurate to the 4th decimal) is obtained by

$$\mu = 1 \times 10^{-5} {}^\circ\text{C}^2 - 6 \times 10^{-4} {}^\circ\text{C} + 0.01787 \text{ for } 0<{}^\circ\text{C}<10 \quad (13)$$

$$\mu = 6.5 \times 10^{-6} {}^\circ\text{C}^2 - 5 \times 10^{-4} {}^\circ\text{C} + 0.01739 \text{ for } 10<{}^\circ\text{C}<20 \quad (14)$$

$$\mu = 4 \times 10^{-6} {}^\circ\text{C}^2 - 4 \times 10^{-4} {}^\circ\text{C} + 0.0164 \text{ for } 20<{}^\circ\text{C}<30. \quad (15)$$

The kinematic viscosity υ is given by μ/ρ.

3.2.2. Classification of fluids

Fluids obey Newton's law of fluids in that the strain rate is proportional to the stress, i.e. they deform continually and permanently while they are being subjected to shear stress. The rate of deformation is measured as the rate of change in length per unit time, which is a function of the fluid viscosity. In Fig. 2, the dynamic viscosity of the fluid between the two plates resists the shear stress produced by the weight. It is expressed as the shear stress divided by the rate of deformation. The shear stress $\tau = F/A = Mg/L^2 = M L^{-1} T^{-2}$, whereas the rate of deformation = velocity gradient $= \delta U/\delta y = L\ T^{-1}/L = T^{-1}$. The dynamic viscosity is thus given by $M L^{-1} T^{-2} T/T^{-1} = M L^{-1} T^{-1}$ (poise).

Fluids are classified according to the ratio of their rate of deformation to the applied shear stress (Fig. 3). Pseudoplastic and dilatant fluids have non-linear ratios decreasing and increasing, respectively, with the applied shear stress. Bingham fluids exhibit a linear ratio, but require a high initial shear stress before they start to deform. Newtonian fluids deform when they are subjected to shear stress (no matter how small) and have linear ratios. Newtonian fluids include liquids and gases, the former displaying a high incompressibility, whereas the latter obeys Boyle's law in that the volume is proportional to the compressive stress.

3.2.3. Classification of fluid flow

Fluid flow is classified in various ways. Laminar flow is characterised by thin laminae gliding along linear paths, with no exchange of mass energy. In turbulent flow, mass energy is dispersed throughout the fluid by turbulent eddies. These types of flow depend on the flow Reynolds number Re_f, which is given by

$$Re_f = \rho d U_m / \mu. \quad (16)$$

The transition from laminar to turbulent flow occurs at a Re_f number of 500–2000 (Reynolds, 1883).

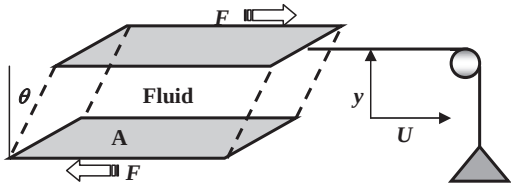

Fig. 2. Schematic diagram to illustrate the concept of dynamic fluid viscosity.

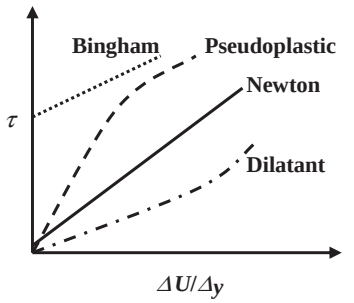

Fig. 3. Different types of fluids.

Subcritical and supercritical flow depend on the Froude number *Fr*, which is given by

$$Fr = U_m / \sqrt{(gd)}. \quad (17)$$

The flow is supercritical when *Fr* is more than 1.

In steady flow, the magnitude and direction of velocity vectors are constant at any specific station over a period of time, whereas during uniform flow, the vectors are constant along the length of a streamline at any specific point in time.

3.2.4. Flow velocity profiles and boundary shear stress

Flow velocity profiles in open channels can consist of a viscous, laminar sub-layer at the base, followed by a boundary or buffer layer and a free or external layer (Fig. 4). A laminar sublayer is only present where Re_f is less than 2000 and the bottom is smooth. The nature of the boundary is determined by the boundary Reynolds number *Re**, which is given by

$$Re^* = \rho k U^* / \mu \quad (18)$$

k being the bed roughness and *U** the shear or friction velocity. The latter cannot be measured directly and is in fact a disguised boundary shear stress (τ_0) with the dimensions of velocity, being given by

$$U^* = \sqrt{(\tau_0/\rho)}. \quad (19)$$

The boundary shear stress is equal to

$$\tau_0 = \rho g d S \quad (20)$$

where *S* is the channel slope (tan of the slope angle α).

If *Re** is less than 5, the boundary is smooth and a viscous sub-layer is present. Where *Re** is 5–65, the boundary is transitional, with turbulence disturbing

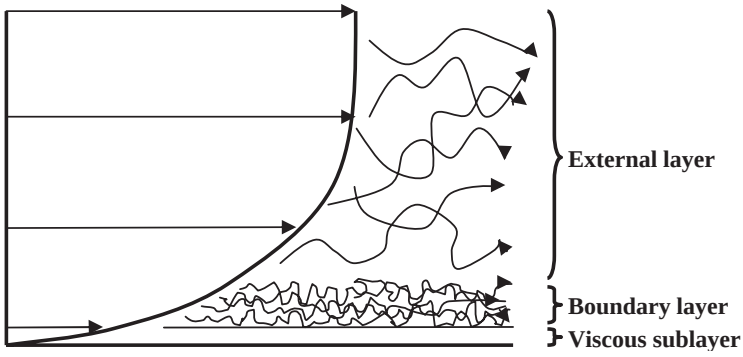

Fig. 4. Components of a typical flow velocity profile.

the viscous sub-layer from time to time. With Re^* higher than 65, the boundary is rough and the flow is turbulent at the bottom. The thickness of the viscous sublayer (∂), which is seldom more than a few mm, is proportional to υ/U^*.

In most shallow rivers the whole profile is a boundary layer, which is characterised by small eddies but very high turbulent and viscous shear stresses. Most of the action takes place in this zone, so that it is very important in terms of sediment transport. An external layer, in which eddies are large and turbulent shear stress dominates over viscous shear stress, can exist in deep rivers. These eddies contain less kinetic energy per unit volume of fluid than the buffer layer.

Vertical velocity profiles are governed by four forms of what is known as the law of the wall. For hydrodynamically smooth boundary conditions where $Re^*<5$, the Prandtl equation is used:

$$U_y = U^*[2.5\ln(\rho U^* y/\mu) + 5.3] \quad (21)$$

where y is the distance from the bottom.

For transitionally rough boundaries ($5<Re^*<65$) over plane beds, Le Roux (2004c) proposed the following equation:

$$U_y = U^*[2.5\ln(Re^* y/D) + 5.3 - 0.1206(Re^* - 5)]. \quad (22)$$

Fully rough boundaries over plane beds have a profile given by the law of the wall for rough boundaries (e.g., Middleton and Southard, 1984):

$$U_y = U^*[2.5\ln(y/D) + 8.5] \quad (23)$$

Over bedforms, an integrated profile (Paola, 1983) is measured at a distance exceeding one or more bedform heights above the crests:

$$U_y = U^*\{2.5\ln[(y - y_a)/y_0]\} \quad (24)$$

where y_a is the displacement height, i.e the distance that the origin must be adjusted to give the highest correlation coefficient on the semi-log velocity profile (Middleton and Southard, 1984) and y_0 is the roughness length, given by the intersection of the adjusted profile with $U=0$.

The mean current velocity U_m is taken as the velocity at $0.37d$, as measured from the bottom. To find the local U^* or τ_0, a velocity profile is measured with a flow meter. The time-averaged U_{av}-values at different depths are plotted on semi-logarithmic paper (Fig. 5).

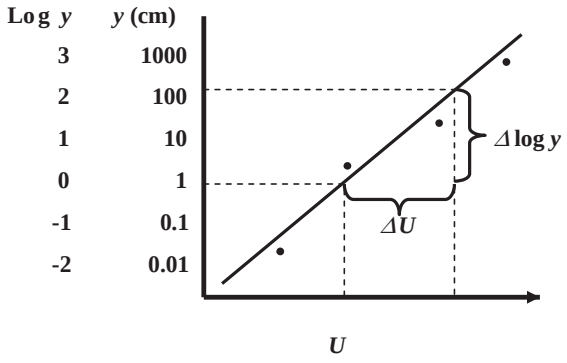

Fig. 5. Determining the boundary shear stress from measured flow velocity profiles.

The relevant relationships are given by:

$$\Delta U_{av}/U^* = (2.3/K)(\Delta \log y), \text{ and}$$
$$U^* = K(\Delta U_{av})/[2.3(\Delta \log y)] \quad (25)$$

where K is the Von Karman constant (0.4 for clear water), and ΔU_{av} and Δy are the differences between U_{1av} and U_{2av} and between y_1 and y_2, respectively.

In practice it is found that the water is very turbulent near the surface, so that most of the measurements are taken near the bottom. U^* is calculated from the best-fit line, after which τ_0 is determined from Eq. (19).

4. Particle settling velocity

4.1. Spherical particles

The settling velocity of a sphere (W_s) with a diameter D_s, is a function of the settling Reynolds number Re_w, where

$$Re_w = \rho D_s W_s/\mu. \quad (26)$$

For Re_w less than about 0.1, Stokes (1851) derived an equation based entirely on theoretical principles, given by

$$W_s = D_s^2 g \rho_\gamma / 18\mu. \quad (27)$$

Newton's impact law, given by

$$W_s = \sqrt{(4\rho_\gamma g D_s/3C_d\rho)} \quad (28)$$

where C_d is a dimensionless drag coefficient, can be used for higher Re_w numbers. However, as W_s is required to determine C_d, it cannot be applied directly.

Empirical equations for Re_w values larger than 0.1 were developed by Rubey (1933), Rouse (1936), Janke (1965), Gibbs et al. (1971), Warg (1973) and Dietrich (1982). Le Roux (1992a,b) used the dimensionless sphere size D_{ds} (Eq. (1)) to determine the dimensionless settling velocity W_{ds} (Eq. (2)). Relating these values to C_d and Re_w it was shown that $\sqrt[3]{(C_d Re_w^2)} = 1.10064 D_{ds}$ and $\sqrt[3]{(Re_w/C_d)} = 0.90856 W_{ds}$. Because the observed dimensionless settling velocities plotted against $1.10064 D_{ds}$ defines segments of nearly straight lines instead of a polynomial curve, 5 equations were proposed to calculate W_{ds} from D_{ds} (Le Roux, 1992a, 1996):

$$W_{ds} = (0.2354 D_{ds})^2 \text{ for } D_{ds} < 1.2538 \quad (29)$$

$$W_{ds} = (0.208 D_{ds} - 0.0652)^{3/2} \text{ for } 1.2538 < D_{ds} < 2.9074 \quad (30)$$

$$W_{ds} = (0.2636 D_{ds} - 0.37) \text{ for } 2.9074 < D_{ds} < 22.9866 \quad (31)$$

$$W_{ds} = (0.8255 D_{ds} - 5.4)^{2/3} \text{ for } 22.9866 < D_{ds} < 134.9215 \quad (32)$$

$$W_{ds} = (2.531 D_{ds} + 160)^{1/2} \text{ for } 134.9215 < D_{ds} < 1750. \quad (33)$$

It can be shown that a coefficient of 0.2357 in Eq. (29) would give exactly the same settling velocity as Stokes law up to a Re_w number of 0.1083, which Le Roux (1992a) considered to represent the limit to which Stoke's Law is accurate. Applying this value would require a slight adjustment in the coefficients of Eqs. (29)–(33), but the final results would differ by almost insignificant factors.

The distinct breaks in slope of the regression lines may be attributed to fluid acceleration, flow separation, and the development of turbulence in the wake of the settling spheres at different Re_w numbers (Le Roux, 1992a).

The sphere settling velocity W_s can be calculated from W_{ds} using Eq. (2). W_{ds} can also be converted to D_{ds} using the following equations:

$$D_{ds} = W_{ds}^{1/2}/0.2354 \text{ for } W_{ds} < 0.0864 \quad (34)$$

$$D_{ds} = \left(W_{ds}^{2/3} + 0.0652\right)/0.208 \text{ for } 0.0864 < W_{ds} < 0.3946 \quad (35)$$

$$D_{ds} = (W_{ds} + 0.37)/0.2636 \text{ for } 0.3946 < W_{ds} < 5.6899 \quad (36)$$

$$D_{ds} = \left(W_{ds}^{3/2} + 5.4\right)/0.8255 \text{ for } 5.6899 < W_{ds} < 22.3967 \quad (37)$$

$$D_{ds} = \left(W_{ds}^2 - 160\right)/2.531 \text{ for } 22.3967 < W_{ds} \quad (38)$$

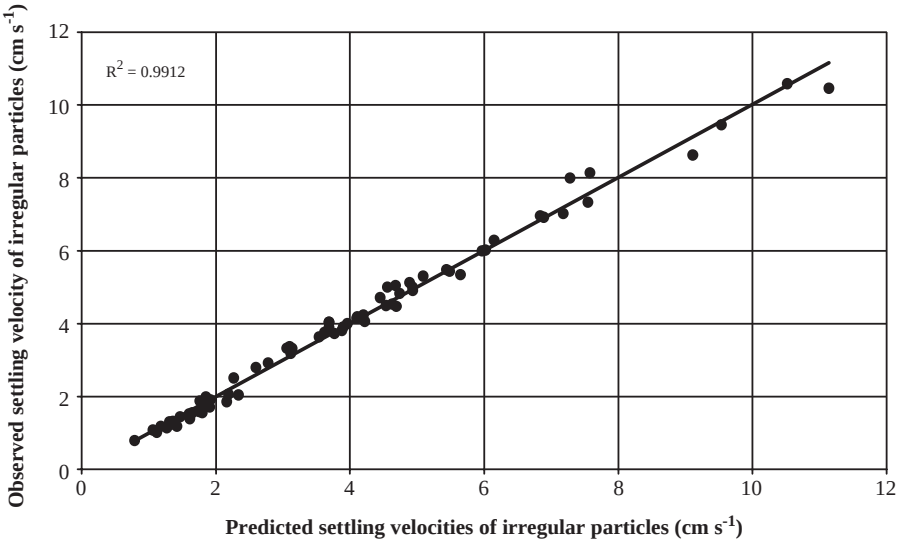

Fig. 6. Comparison of measured settling velocities of irregular particles and settling velocities predicted by Eq. (39), based on the experimental results of Baba and Komar (1981a).

From D_{ds}, D_s can be found using Eq. (1).

As these equations are all based on dimensionless numbers, they are valid for all Newtonian fluids, including air (Le Roux, 2002c, 2005). For the data of Gibbs et al. (1971), they produce mean and maximum errors of 1.1% and 2%, respectively.

4.2. Non-spherical particles

Since the pioneering work of Wadell (1932) and Rubey (1933), many researchers have studied the effect of grain shape on particle settling velocity. The shape indices most frequently applied include those of Wadell (1932), Corey (1949) and Janke

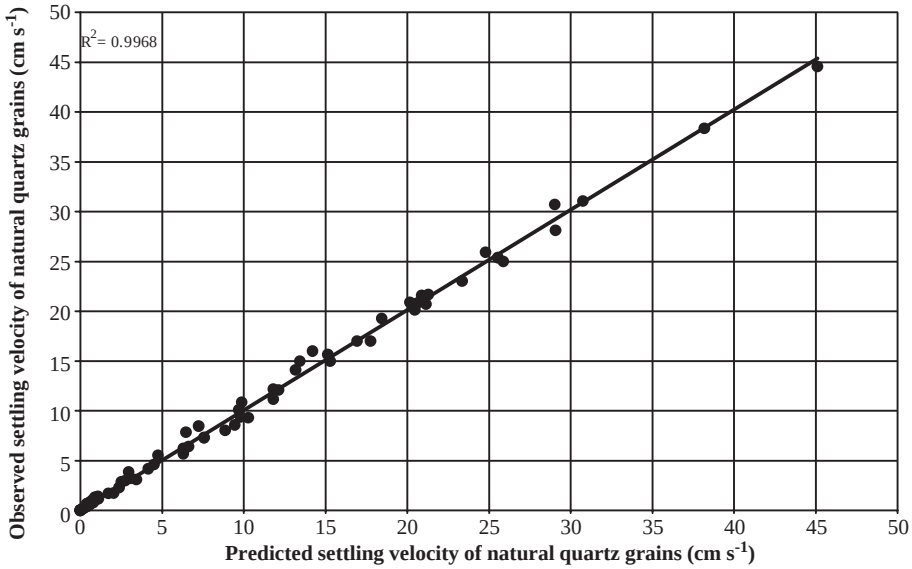

Fig. 7. Comparison of measured settling velocities and settling velocities of natural grains predicted by Eq. (39), based on the experimental results reported by Cheng (1997), Hallermeier (1981), and Ferguson and Church (2004).

Table 1
Comparison of settling velocity predictions using Eqs. (39) and (42), and the next best available equation

Shape	Max. Re_w	z	ME%	a	b	ME%	ME%
Ellipsoid	1.363	2.5	3.6	0.5833	0.4167	4.2	5.5 (K and R, 1978)
Spheroid	117,992	0.7	1.4	0.5833	0.4167	2.9	3.2 (D, 1982)
Prolate spheroid	57,200	2.0	3.1	0.6055	0.3945	3.2	3.7 (D, 1982)
Oblate spheroid	508	1.3	3.7	0.8456	0.1544	3.5	4.0 (D, 1982)
Oblate spheroid	4150	0.8	2.9	0.8929	0.1071	4.3	2.0 (D, 1982)
Disc	249.2	1.6	4.5	0.5407	0.4593	4.8	–
Cylinder/rod	1.438	2.8	1.8	0.1089	0.8911	3.8	3.8 (K, 1980)
Cylinder/rod	308	2.0	2.7	0.34	0.66	2.8	19.7 (D, 1982)
Natural grains	5810.6	–	–	0.813	0.187	4.9	5.4 (Z and C, 1993)

K=Komar, 1980; K and R=Komar and Reimers, 1978; D=Dietrich, 1982; Z and C=Zhu and Cheng, 1993.

(1966), on which the settling equations of Komar and Reimers (1978), Baba and Komar (1981a) and Dietrich (1982) were based. The Dietrich equation has probably been used most widely.

Le Roux (1996) used the Hofmann (1994) shape entropy (Eq. (8)) in the following procedure to calculate the settling velocity. First, the dimensionless equivalent sphere size D_{ds} is calculated from Eqs. Eqs. (29–(33)). W_s is then calculated from Eq. (2). The settling velocity W_p of ellipsoids is predicted using the following relationship:

$$W_p = W_s[H_r - a]/b \quad (39)$$

where $a+b=1$, a being 0.5833 and $b=0.4167$ for ellipsoids.

Applied to the data set of Komar and Reimers (1978), a mean error of 4.2% was obtained, compared to 5.3%, 5.5% and 9.6% for the equations of Dietrich (1982), Komar and Reimers (1978) and Baba and Komar (1981a).

Le Roux (1997a) subsequently compared 6 of the most widely used shape indices (Wadell, 1932; Krumbein, 1941; Corey, 1949; Aschenbrenner, 1956; Sneed and Folk, 1958; Janke, 1966) with that of Hofmann (1994), normalising the original values to allow direct comparison. The most suitable index for settling velocity prediction turned out to be that of Hofmann (1994), followed by Aschenbrenner (1956) and Wadell (1932). In subsequent papers, Le Roux (2002a,b) showed that the Hofmann shape entropy

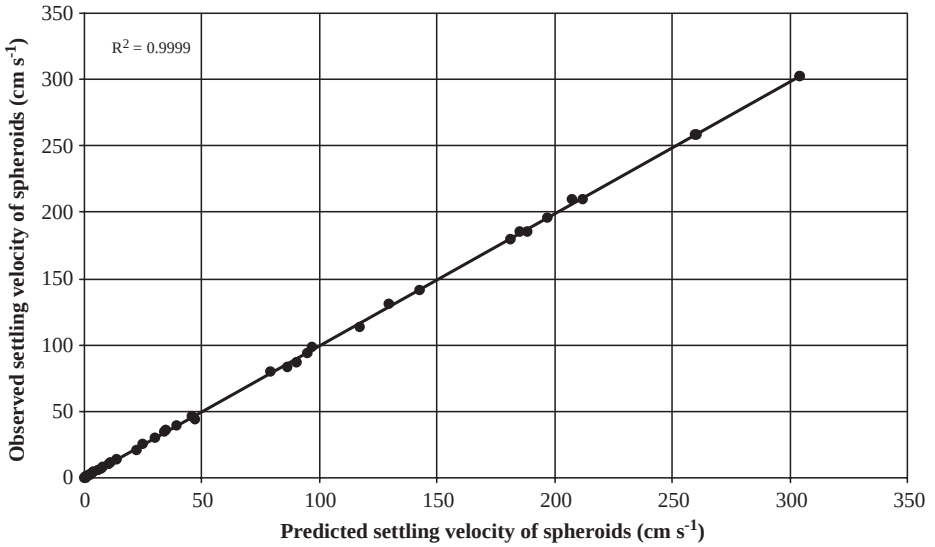

Fig. 8. Comparison of measured settling velocities of spheroids and settling velocities predicted by Eq. (42), based on the experimental results of Williams (1966), Stringham et al. (1969) and Gibbs et al. (1971).

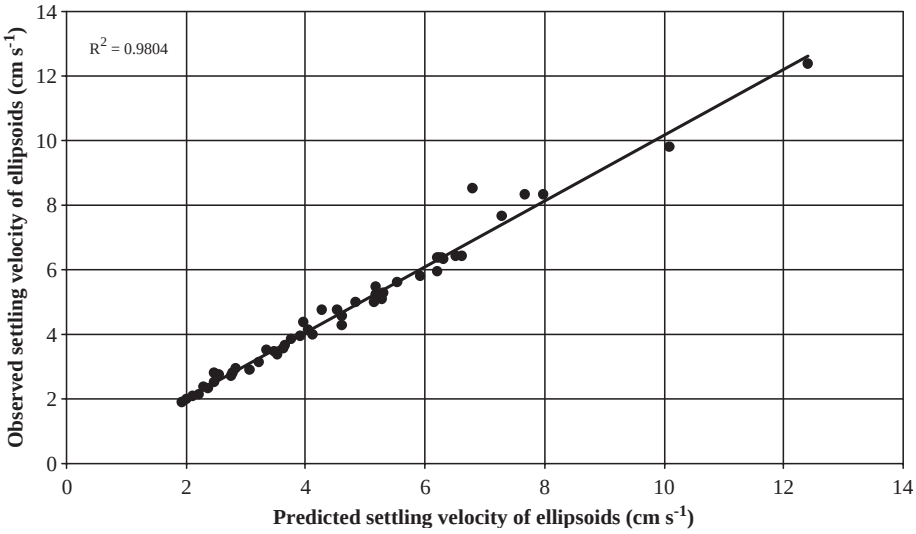

Fig. 9. Comparison of measured settling velocities of ellipsoids and settling velocities predicted by Eq. (42), based on the experimental results of Komar and Reimers (1978).

method can be adapted for irregular, semi-ellipsoidal grains as well as natural grains. For the first case, $a=0.23$ and $b=0.77$ in Eq. (39), giving a mean error of 5.2% for the data set of Baba and Komar (1981a) on beach glass fragments (Fig. 6). For natural grains, with $a=0.813$ and $b=0.187$ in Eq. (39), a mean error of 4.9% was obtained, based on different data sets reproduced in Cheng (1997). The shape entropy H_r of

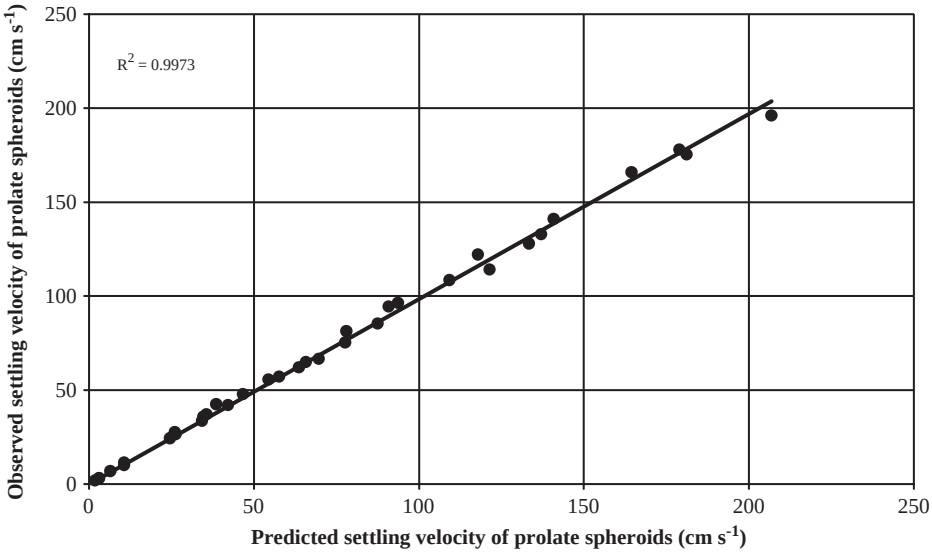

Fig. 10. Comparison of measured settling velocities of prolate spheroids and settling velocities predicted by Eq. (42), based on the experimental results of Williams (1966), Stringham et al. (1969) and Komar (1980).

natural grains is given by the following expressions (Le Roux, 2002b):

$$H_r = -100.13D_n^3 + 3.6533D_n^2 + 0.7515D_n + 0.8903 \text{ for } D_n<0.065 \quad (40)$$

$$H_r = -0.0631D_n^3 + 0.18D_n^2 - 0.1473D_n + 0.9437 \text{ for } D_n>0.065. \quad (41)$$

In Fig. 7, additional data sets of Hallermeier (1981) and Ferguson and Church (2004) have now been added, which confirm the validity of Eqs. (39)–(41). Eq. (39) gives a mean absolute error of 11.6% for this expanded data set, compared to 13.1% for the latest equation proposed by Ferguson and Church (2004).

Le Roux (2004b) examined the effect of using different axial ratios on grains with stable settling patterns, finding that the ratio D_m/D_l shows the best correlation with the settling velocity. He used a modified hydrodynamic shape index, $[1-(D_m/D_l)]^z$, derived from Eq. (10), to define a settling equation for differently shaped grains:

$$W_p = -W_s\{0.572[1-(D_m/D_l)]^z - 1\} \quad (42)$$

This was based on the nominal grain size D_n, from which the settling velocity of the equivalent sphere W_s was calculated using Eqs. (29)–(33). The value of z was found to vary for different grain shapes, as shown in Table 1. Figs. 8–13 compare the observed and predicted settling velocities of spheroids, ellipsoids, oblate and prolate spheroids, discs, cylinders, and rods for different data sets. Eq. (39), based on the Hofmann shape entropy, was also found to give good results, provided that the values of x and y are varied as shown in Table 1. The mean errors (ME) of Eqs. (39) and (42) are compared with that of the next best equation (last column), based on the data sets of Williams (1966), Stringham et al. (1969), Komar and Reimers (1978) and Komar (1980).

Based on these results, Le Roux (2004b) proposed a hydrodynamic classification of grain shapes, as shown in Table 2.

5. Particle entrainment

Entrainment takes place when the critical boundary shear stress τ_c for a particle is exceeded. This depends on factors such as the grain size, shape and density, the boundary roughness, the internal friction or pivot angle ϕ, the bedslope angle α, and the flow velocity U_y. The latter is controlled by the type of flow (unidirectional or oscillatory, laminar or turbulent).

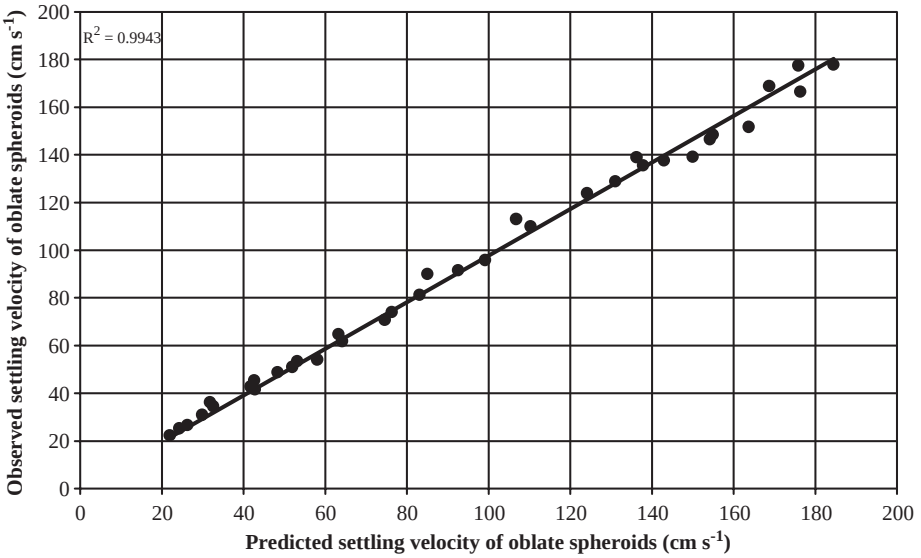

Fig. 11. Comparison of measured settling velocities of oblate spheroids and settling velocities predicted by Eq. (42), based on the experimental results of Stringham et al. (1969).

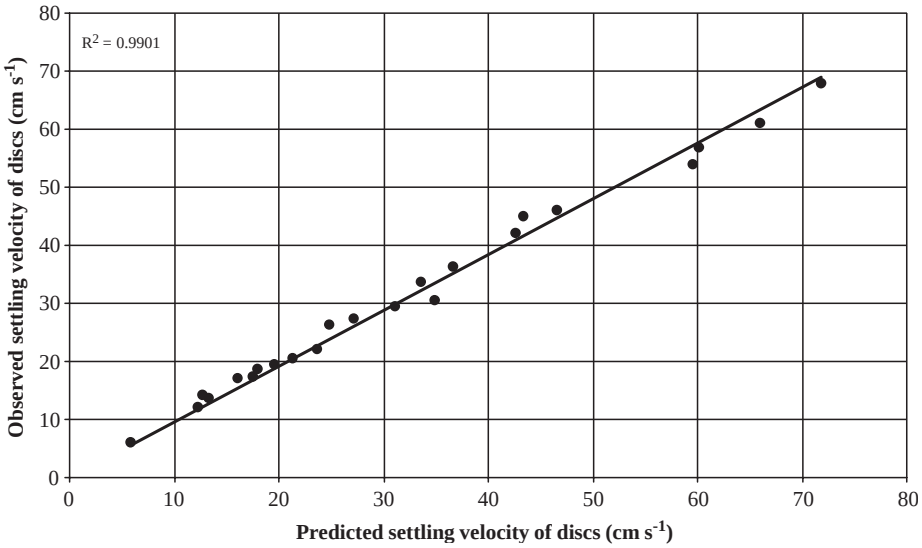

Fig. 12. Comparison of measured settling velocities of discs and settling velocities predicted by Eq. (42), based on the experimental results of Williams (1966) and Stringham et al. (1969).

5.1. Entrainment on horizontal plane beds

5.1.1. Unidirectional currents: water and other liquids

Numerous empirical equations have been proposed to predict the threshold of sediment entrainment in water (Hjulstrom, 1935, 1939; Shields, 1936; Inman, 1949; Lane, 1955; Sundborg, 1956; Bagnold, 1963; Vanoni, 1964; Graf, 1971; Miller and Komar, 1977; Miller et al., 1977; Yalin, 1977; Yalin and Karahan, 1979; Le Roux, 1991b, 1997c; Niño et al., 2003). A more theoretical approach was pursued by others such

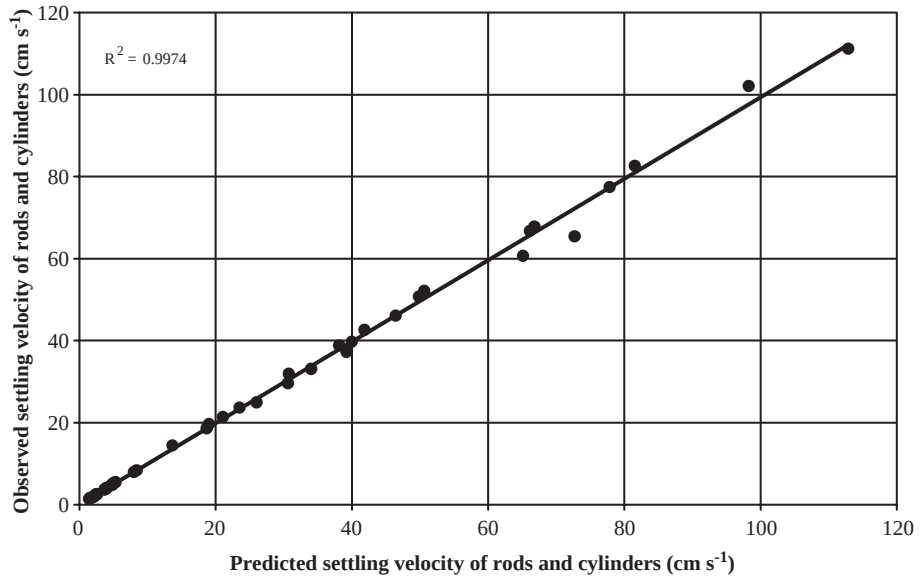

Fig. 13. Comparison of measured settling velocities of cylinders and rods and settling velocities predicted by Eq. (42), based on the experimental results of Stringham et al. (1969) and Komar (1980).

Table 2
Hydrodynamic classification of grain shapes (Le Roux, 2004b)

Shape	D_s/D_i	D_i/D_l
Spheroid	0.9–1	0.9–1
Ellipsoid	0.35–0.9	0.35–0.9
Prolate spheroid	0.9–1	0.35–0.9
Oblate spheroid	0.35–0.9	0.9–1
Disc	0–0.35	0.9–1
Cylinder/rod	0.9–1	0–0.35

as Allen (1982a,b), Wiberg and Smith (1987), Bridge and Bennett (1992), and Soulsby and Whitehouse (1997), who evaluated the balance of forces on individual particles at the bed surface. Many of these studies use the dimensionless critical boundary shear stress β_c of Shields (1936):

$$\beta_c = \tau_c/\rho_\gamma g D. \quad (43)$$

The dimensionless critical boundary shear stress can be used to calculate the critical shear velocity U_c^*, as follows:

$$U_c^* = \sqrt{(\beta_c g D \rho_\gamma/\rho)}. \quad (44)$$

Le Roux (1998) related the dimensionless settling velocity of sieve-size spheres (W_{dv}) to their transport threshold in unidirectional currents in liquids, following earlier attempts to do so by Collins and Rigler (1982), Komar and Clemens (1985) and Bridge and Bennett (1992). In a previous paper, Le Roux (1991b) showed that Re^* and β_c are related to the non-dimensional grain size D_d in the following way:

$$D_d = \sqrt[3]{\left(Re^{*2}/\beta_c\right)}. \quad (45)$$

From this relationship, Le Roux (1998) determined the dimensionless equivalent sieve-size spheres (D_{dv}) for data plotted by Yalin and Karahan (1979) on a Re^* vs. β_c diagram. Using Eqs. (29)–(33), these data were then recast in a plot of β_c against W_{dv}, including the data of Paintal (1971), Everts (1973) and Govers (1987). This yielded the following relationship between W_{dv} and β_c:

$$\beta_c = -0.0717\log_{10}W_{dv} + 0.0625 \text{ for } W_{dv}<2.5 \quad (46)$$

$$\beta_c = 0.0171\log_{10}W_{dv} + 0.0272 \text{ for } 2.5<W_{dv}<11 \quad (47)$$

$$\beta_c = 0.045 \text{ for } W_{dv}>11 \quad (48)$$

Eqs. (46)–(48)) are valid for Re^* numbers between 0.03 and at least 1000.

5.1.2. Unidirectional currents: air or other gases

Le Roux (1997b), following on earlier investigations on the threshold of transport in wind (Bagnold, 1941; Zingg, 1953; Chepil, 1959; Miller et al., 1977; Iversen and White, 1982; Williams et al., 1994), concluded that the dimensionless critical threshold of particles (β_c) in wind is related to the dimensionless settling velocity of their equivalent sieve diameter spheres (W_{dv}) in water in the following way:

$$\beta_c = -0.00741\log_{10}W_{dv} + 0.01495 \text{ for } 0.004<W_{dv}<2.5 \quad (49)$$

$$\beta_c = 0.00664\log_{10}W_{dv} + 0.00936 \text{ for } 2.5<W_{dv}<10. \quad (50)$$

Eqs. (49) and (50) are valid for quartz grain sizes between 0.001 cm and at least 0.166 cm at temperatures between −50 and 40 °C. Fig. 14 compares the measured critical shear stress for wind with the critical shear stress predicted by Eqs. (49) and (50).

5.1.3. Oscillatory waves: water or other liquids

The threshold of sediment entrainment under oscillatory waves has been studied by, inter alia, Bagnold (1946), Manohar (1955), Rance and Warren (1969), Komar and Miller (1973, 1975a), Madsen and Grant (1975), Sleath (1977), Hammond and Collins (1979), Rigler and Collins (1983) and Soulsby and Whitehouse (1997). Sediment motion commences when the critical orbital velocity U_{wc} of the wave is exceeded, with the wave orbital velocity U_w related to the critical oscillatory bed shear stress τ_{wc} as follows:

$$\tau_{wc} = 0.5\rho f_{dw} U_w^2 \quad (51)$$

where f_{dw} is a dimensionless wave friction factor or drag coefficient.

Le Roux (2001a,b) defined a dimensionless wave orbital velocity as:

$$U_{dw} = U_w(\rho\mu/T_w)^{0.5}/gD\rho_\gamma. \quad (52)$$

Plotting the dimensionless critical wave orbital velocity U_{dwc} against the dimensionless settling ve-

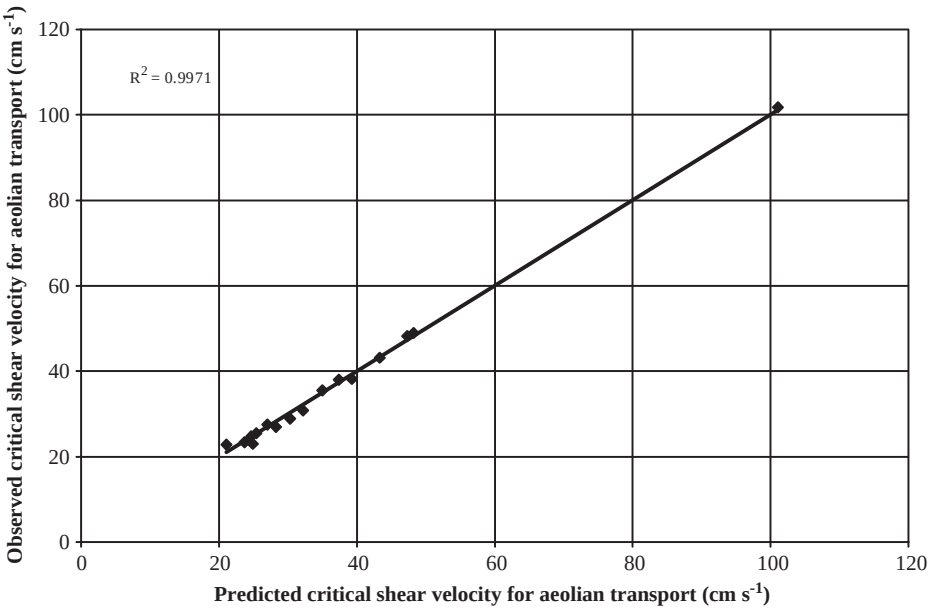

Fig. 14. Comparison of observed critical shear velocity for wind and shear velocity predicted by Eqs. (49) and (50), based on the experimental results of Iversen and White (1982) and Nickling (1988).

locity W_{dv} for the data sets of Bagnold (1946) and Manohar (1955), the following relationship was established:

$$U_{dwc} = 0.0246 W_{dv}^{-0.55} \tag{53}$$

U_{wc} is given by

$$U_{wc} = -0.01\left[\left(U_{dwc} g D \rho_\gamma\right)^2/(\rho\mu/T_w)\right] + 1.3416\left[\left(U_{dwc} g D \rho_\gamma\right)/(\rho\mu/T_w)^{0.5}\right] - 0.6485 \text{ for } U_{wc}<50\,\text{cm s}^{-1}. \tag{54}$$

In reply to a discussion by You and Yin (2004), Le Roux (2004a,e) added the data set of Rance and Warren (1969) for coarse grains, showing that

$$U_{dwc} = 0.027 W_{dv}^{-0.6757} \tag{55}$$

and

$$U_{wc} = -0.002\left(U_{dwc}^2 g^2 D^2 \rho_\gamma^2 T_w/\rho\mu\right) + 1.0702\left[U_{dwc} g D \rho_\gamma (T_w/\rho\mu)^{0.5}\right] \tag{56}$$

give good results for orbital velocities up to 150 cm s^{-1} (Fig. 15).

The wave friction factor f_{dw} can also be related to the Shields parameter β_c for steady currents, (Le Roux, 2002d), which provides a direct link between sediment entrainment by waves and currents. It can be argued that the motion of water particles beneath a wave is essentially horizontal at the level of sediment grains resting on a flat bed. The critical oscillatory bed shear stress τ_{wc} can therefore be equated with τ_c for steady currents, as both depend on the same balance of forces. Combining Eqs. (43) and (51), this leads to:

$$f_{dw} = 2\tau_c U_{wc}^2 = 2\beta_c g D \rho_\gamma / U_w^2 \rho. \tag{57}$$

Using Eqs. (46)–(48) to determine β_c and Eq. (56) to find U_{wc}, f_{dw} is therefore easily determined. This allows τ_{wc} and τ_c to be added

$$\tau_t = \tau_{wc} + \tau_c \tag{58}$$

so that the combined effect of currents and waves on the initiation of sediment transport can be examined.

5.2. Entrainment on inclined plane beds

Theoretical calculations of entrainment thresholds on sloping beds (Allen, 1982b; Dyer, 1986; Soulsby and Whitehouse, 1997) all require the pivot angle ϕ, but each of these authors used different values for ϕ.

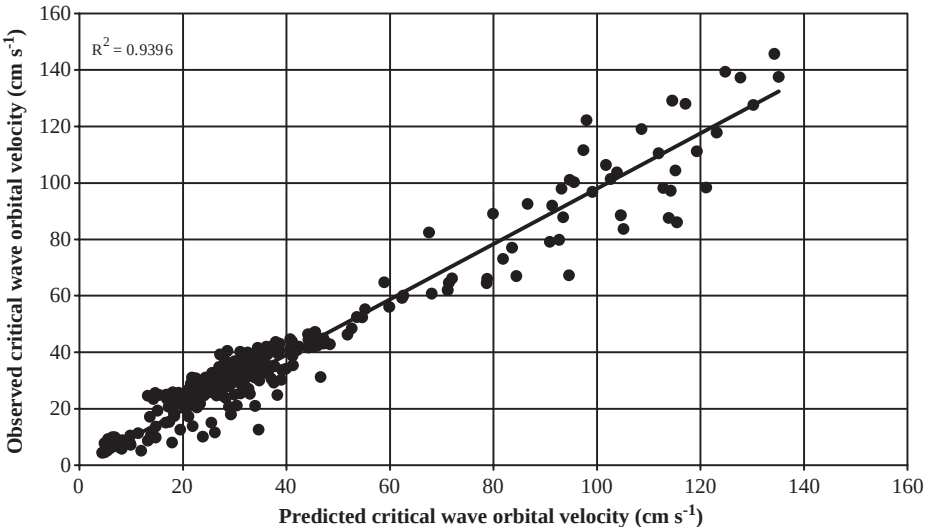

Fig. 15. Plot of measured critical wave orbital velocity and critical wave orbital velocity as predicted by Eqs. (55) and (56), based upon the experimental results of Bagnold (1946), Manohar (1955), Hammond and Collins (1979) and Rance and Warren (1969).

Two of these studies employed the ratio between the critical flow velocity on the slope ($U_{c\alpha}$, with α denoting the slope angle taken as positive upward in the direction of flow) and the corresponding value on a horizontal bed (U_c).

According to Allen (1982b):

$$U_{c\alpha}/U_c = 1.3204\sqrt{[\sin(\phi+\alpha)]} \tag{59}$$

where ϕ was taken as 35°, noting that Allen's original equation is modified here to account for the fact that he measured the bed slope α positively downward in the direction of flow, as opposed to the convention followed here. The coefficient in Eq. (59) in fact depends on the value chosen for ϕ, being given by $1/\sqrt{sin\phi}$.

Dyer (1986) developed the following equation from theoretical considerations:

$$U_{c\alpha}/U_c = \sqrt{\{\cos\alpha[(\tan\phi+\tan\alpha)/\tan\phi]\}} \tag{60}$$

with ϕ taken as 30°. Eqs. (59) and (60) give the same results if the same pivot angle is used.

The method of Soulsby and Whitehouse (1997) differs from the previous two techniques in using the dimensionless critical shear stress β_c:

$$\beta_{\alpha c}/\beta_c = \sin(\phi+\alpha)/\sin\phi \tag{61}$$

the subscripts α and c having the same meaning as before and ϕ taken by Soulsby and Whitehouse as 32°.

Allen (1982b) and Soulsby and Whitehouse (1997) used different methods to calculate U_c and β_c, but Allen's equation contains variables that cannot be defined or measured accurately, whereas the Soulsby and Whitehouse equation is rather inaccurate in the range of grains coarser than about 0.08 cm. However, using Eqs. (1),(29) (30) (31) (32) (33) and (46) (47) (48) above, β_c can be calculated from the mean sediment size. To determine the critical flow velocity from β_c at any distance y above the bed, the appropriate form of the law of the wall (Eqs. (21)–(23)) is used, once U_c^* and Re^* have been calculated from Eqs. (44) and (18).

A set of experiments investigating sediment entrainment on sloping beds was conducted by Whitehouse and Hardisty (1988), who used well-rounded quartz sand and measured the average flow velocity at threshold 0.5 cm above the bed. Twenty-four experiments were conducted for each of 28 bedslopes varying by increments of 2° from −24° to 32° The critical flow velocity 0.5 cm from the bed ($U_{c0.5}$) is given by a curve fitted through the data (Fig. 16):

$$U_{c0.5} = 0.0009\alpha^3 - 0.0234\alpha^2 + 0.0645\alpha + 36.476. \tag{62}$$

Because the mean grain size of the sand was not supplied by Whitehouse and Hardisty (1988), the

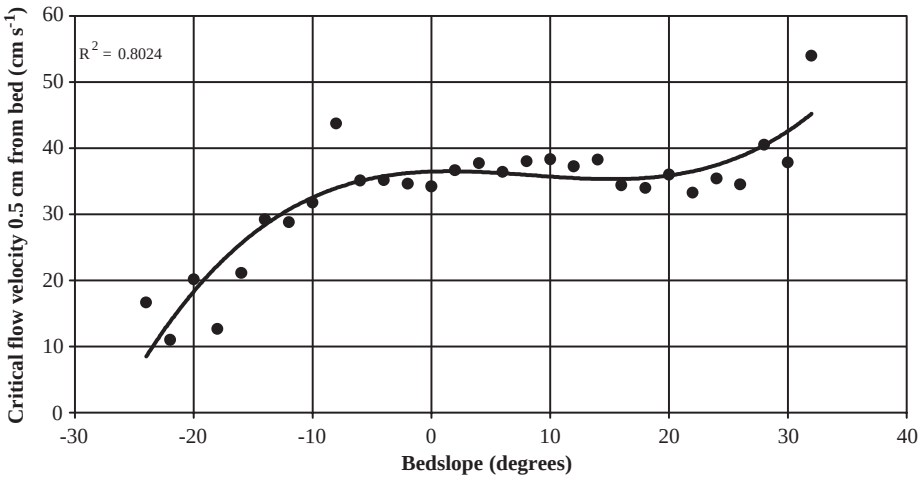

Fig. 16. Plot of critical flow velocity against bed slope α.

given critical flow velocity on a horizontal bed (34.23 cm/s) was employed to calculate D_*. Using a value of 981 cm s^{-2} for the gravity constant, 0.99821 g cm^{-3} and 0.01 g $cm^{-1}s^{-1}$ for the density and dynamic viscosity of water at 20 °C (Eqs. (11) and (14)), respectively, and 2.65 g cm^{-3} for the grain density, the grain size required to yield a threshold flow velocity of 34.23 cm on a horizontal bed was found by inspection to be 0.0764 cm, with the corresponding values of β_c and U_c^* being 0.0387 and 2.1908 cm s^{-1}, respectively.

Inserting this value of β_c into Eq. (61) for different values of ϕ and α, $\beta_{c\alpha}$ can be determined, as well as the corresponding U_c^* and Re_c^* values for different bedslopes. In this case, Re_c^* in all cases lies between 5 and 65. Eqs. (44) and (22) are therefore used to calculate the threshold flow velocity at 0.5 cm ($U_{c\alpha 0.5}$) on the sloping beds. The best value for the internal friction angle ϕ can be determined by comparing the critical flow velocity given by Eq. (62) with the threshold velocities predicted by the models of Allen (1982b) and Soulsby and Whitehouse (1997). The value of ϕ was varied from 45° to 25° for each of the methods, while calculating the mean of the prediction error (ME) expressed as a percentage:

$$\mathrm{ME} = 100\left[\left(U_{\mathrm{observed}} - U_{\mathrm{predicted}}\right)/U_{\mathrm{observed}}\right]. \qquad (63)$$

The lowest ME is obtained with a pivot angle of 31°, being 13.26% if the method of Allen (1982b) is used with the corresponding coefficient of 1.3934 in Eq. (59). Calculating the threshold flow velocities from the law of the wall for transitional boundaries Eq. (22) together with the appropriate values of Re_c^* and U_c^* as computed for different values of α, gives an ME of 13.06% (15.45% if the raw data are used instead of Eq. (62)). Using the appropriate of Eqs. (21)–(23) thus allows the critical flow velocity to be determined at any distance y from the bed on any slope angle.

6. Transport rate of sediments

6.1. Bedload discharge

Sediment transport takes place when certain critical or threshold values are exceeded, which may include the critical shear velocity U_c^*, the critical boundary shear stress τ_c, or the mean current velocity at the threshold of sediment transport U_{mc}. Numerous bedload transport equations have been proposed (for reviews, see Graf, 1971; Yalin, 1977; Chang, 1988; Bridge and Bennett, 1992; Wilcock, 1993; Van Rijn, 1993; Bennett, 1995; Buffington and Montgomery, 1997), based on both empirical and theoretical approaches. Many of these methods are based on the skin friction, i.e. local shear stress exerted on the granular bed surface at a particular point. In the case of bedforms, the skin friction varies from trough to crest, which makes this approach impractical for nat-

ural conditions because it would be very difficult to know exactly where a velocity profile is situated. Moreover, as bedforms are in continuous motion, the skin friction would vary over time as the bedform migrates under the measured profile. A more practical approach would therefore be to use integrated profiles (Paola, 1983), which characterize layers of the flow that blanket entire fields of bedforms without varying at the scale of the latter (Middleton and Southard, 1984).

Le Roux (2004c) proposed a method based on the excess stream power principle of Bagnold (1963), i.e. the difference between the available stream power and the stream power required to entrain the sediment. Equations of this nature have been published before (e.g. Meyer-Peter and Muller, 1948; Ashida and Michiue, 1973; Luque and Van Beek, 1976; Miller et al., 1977; Engelund and Fredsoe, 1976; Hardisty, 1983; Wang and Gao, 2001), but unfortunately not always with very good results. (See Wang and Gao, 2001; Le Roux, 2004c). The Le Roux (2004c) equation, given by

$$q_{bp} = 3.284 \times 10^{-6}\left(U_m^2 - U_{mc}^2\right)U_m \qquad (64)$$

is applicable to sediment transport over plane beds, where q_{bp} is the predicted bedload transport rate or discharge in g cm^{-1} s^{-1}, U_m is the mean flow velocity and U_{mc} is the mean flow velocity at the threshold of sediment motion, in cm s^{-1}. A correlation coefficient R^2 of 0.9787 was obtained between the predicted and observed bedload transport rates for 31 runs over plane beds recorded by Guy et al. (1966). Eq. (64) is not dimensionally correct, however.

Le Roux (2004d) and Le Roux and Brodalka (2004) applied a related methodology to runs over bedforms, based on an expanded data set of Guy et al. (1966), who summarized the data from numerous flume experiments carried out between 1956 and 1961 at the Colorado State University. Two recirculating flumes, 244 and 61 cm wide, were used, with runs over natural sand having median fall diameters (D_w) of 0.019, 0.027, 0.028, 0.032, 0.033, 0.045 and 0.093 cm. Other runs with grain fall diameters of 0.047 and 0.054 cm where bentonite had been added to the water to increase the viscosity, were also analyzed, using the values of the friction velocity U^* and the boundary shear stress τ_0 supplied by Guy et al. (1966), to calculate the fluid density ($\rho = \tau_0 / U^{*2}$). The fall diameters were converted to equivalent sieve diameters (D_v) based on their settling velocities as influenced by the Hoffman shape entropy (Le Roux, 2002b; Le Roux and Brodalka, 2004), yielding sieve diameters of 0.0225, 0.0307, 0.0318, 0.0362, 0.0373, 0.0515, 0.054, 0.0632 and 0.1303 cm. Sorting of the sand was generally poor, ranging from 1.3 to 2.07 and most likely accounting for most of the data scatter.

Middleton and Southard (1984) recommended that velocity profiles over bedforms should start 1 to 2 ripple heights above the crests, and as Guy et al. (1966) only reported distances above the bed, a minimum distance of 2.5 times the bedform amplitude was taken in this case. This ensured that, even in the case of profiles having been measured above bedform troughs, a distance of at least 1.5 times the bedform height above the crests was used as the lowest reading on the profile. Many of the runs were thus eliminated, as a minimum of 4 velocity readings were considered appropriate for each run.

The origin of the regression line was juggled up and down to give the best semi-log straight line fit for these data points (Middleton and Southard, 1984). R^2 values for the regression lines in all cases exceeded 0.95, with 77% of the R^2 values exceeding 0.99. This ensured that only the most reliable runs were employed. Of the total of 74 runs analyzed, 40 were over plane beds, 26 over ripples and 4 over each of what is here classified as short- and long-wavelength dunes, respectively. Few runs could be analyzed over dunes due to the shallow water depths employed, which did not allow for 4 or more velocity measurements to be obtained.

The mean flow velocity was taken at 0.37 times the flow depth from the bottom (Bridge and Bennett, 1992), calculating it from the velocity profile after straightening out the latter, whereas the mean velocity at the threshold of sediment motion was determined using Eqs. (1),(29) (30) (31) (32) (33),(46) (47) (48),(44) and (21) (22) (23) (24). To calculate the shear velocity U^*_{calc}, Le Roux and Brodalka (2004) iterated the value of U^* while summing the differences between the observed and theoretical velocity given by the appropriate of Eqs. (21)–(24), at every height y from the bed, until the smallest difference between the two profiles was obtained.

Experimenting with the parameters involved in bedload transport indicated that the main controlling variables are the fluid density ρ, the mean flow velocity U_m, the median sieve size D_v, the grain submerged density ρ_γ, the gravity acceleration g, and the type of bedform C. The bed slope S is accounted for by using Eq. (61) to calculate the value of $\beta_{c\alpha}$ from β_c (converting S to the bedslope angle α). The water depth d partly controls the mean flow velocity and is thus integrated into U_m and U_{mc}. The critical mean velocity U_{mc} is based on the dimensionless settling velocity W_{dv} of the dimensionless median sediment size D_{dv}, which takes into account both fluid and sediment properties (including shape). Calculation of U_{mc} also considers flow properties such as the dimensionless critical boundary shear stress β_c, as well as the boundary Reynolds number Re^* and the hydrodynamic boundary conditions. The bedload discharge q_b can therefore be considered to be a function of the variables C, ρ, ρ_γ, μ, U_m, U_{mc}, and g. Using Buckingham's Pi-theorem (as explained in Section 2), these variables were combined into a dimensionally correct bedload equation (Le Roux, 2004d):

$$q_{bp} = C\rho^2\left(U_m^3 - U_{mc}^3\right)/g\rho_\gamma \qquad (65)$$

where q_{bp} is in g cm^{-1} s^{-1}.

Plotting this relationship for different bedforms indicates that $C = 5.003 \times 10^{-3}$ for plane beds ($R^2 = 0.974$), 2.256×10^{-3} for ripples ($R^2 = 0.9291$), and 1.65×10^{-3} for short-wavelength dunes ($R^2 = 0.9517$). The equations work well for runs with a bedload discharge of up to about 10 g cm^{-1} s^{-1}, but for higher transport rates widely discrepant results are obtained.

Eq. (65) can be improved somewhat for ripples and dunes, by fitting a polynomial curve to its results.

$$q_{bp} = -8.11X^3 + 4.7697X^2 - 0.4287X \qquad (66)$$

where X is the bedload discharge given by Eq. (65). R^2 in this case is 0.9537.

Four runs over long-wavelength dunes were also analyzed, giving a value of 3.12×10^{-3} for C with a correlation coefficient of 0.7374. However, as the last result is based on only four runs yielding a relatively poor correlation coefficient, it is given here only for the sake of interest. Fig. 17 plots the predicted against the observed bedload transport rates for all runs (plane beds, ripples and dunes). The correlation coefficient between predicted and observed bedload transport rates is 0.9801.

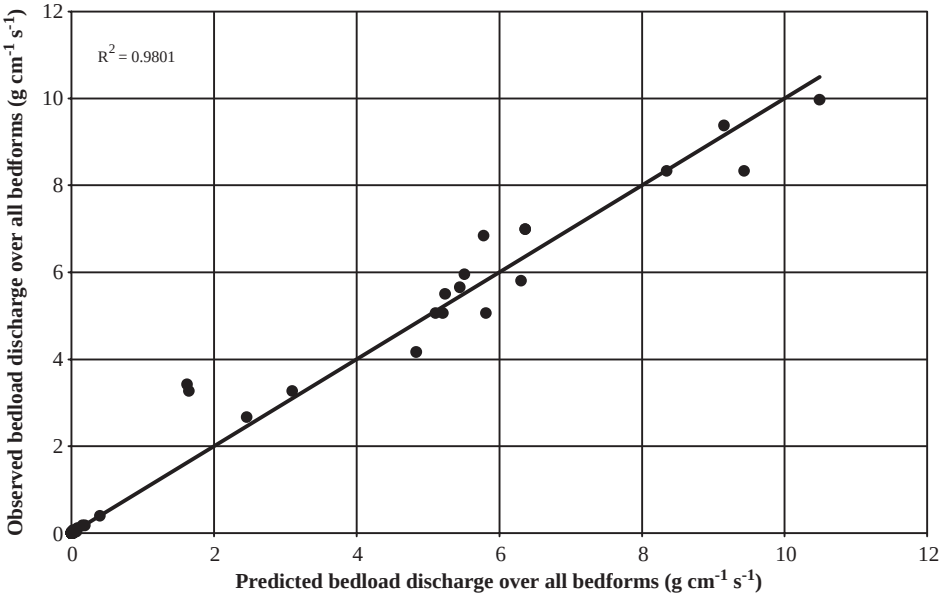

Fig. 17. Plot of observed bedload discharge over all bedforms against discharge predicted by Eq. (65), based upon the experimental results of Guy et al. (1966).

An analysis of the data indicates that the limit between ripples and dunes (where an exponent of either 2.256×10^{-3} or 1.65×10^{-3} must be used) is at a ripple wavelength λ of about 50 (although one run with a λ value of 51.8 still gave good results with $C=2.256\times10^{-3}$). Allen (1982a) considered dunes to have a wavelength of more than 60 cm and amplitudes exceeding 4 cm, but this is apparently not supported by their hydrodynamic behaviour. The ripple amplitude H does not seem to be very important in governing sediment transport, as H varied from 0.61 to 2.14 cm for ripples and from 0.61 to 1.83 cm for short-wavelength dunes (as classified here). The ripple index λ/H ranged from 10 to 43 for ripples and from 48 to 145 for dunes. The limit between dunes and long-wavelength dunes lies at a λ of about 100, 88.39 being the highest for which $C=1.65\times10^{-3}$ still gives the best results, and 106.7 being the lowest λ for which $C=3.12\times10^{-3}$ gives better results. H varied from 1.52 to 5.49 for long-wavelength dunes, with λ/H ranging between 19 and 74. According to the classical subdivision of dunes and sand waves (Allen, 1982a), these bedforms can therefore not be considered as true sand waves. More studies are required to determine whether the difference in transport behaviour is consistent for different wavelength bedforms, but it seems as if a hydrodynamic classification is required instead of the present arbitrary scheme.

6.2. Suspended load discharge

It is generally agreed that grains go into suspension when the shear velocity U^* exceeds their settling velocity W (Bagnold, 1966; Middleton and Southard, 1984), or a certain function of their settling velocity (Van Rijn, 1984; Niño et al., 2003). Le Roux and Brodalka (2004) tested this concept by plotting the observed suspension loads over 33 plane bed runs (Guy et al., 1966) against an "excess shear velocity" given by $(U^*_{\mathrm{calc}}-W_{\mathrm{v}})$. This led to a dimensionally correct equation of the form:

$$q_{\mathrm{sp}}=7003.7\left[\rho\mu\left(U^*_{\mathrm{calc}}-W_{\mathrm{v}}\right)/\rho_{\gamma}U_{\mathrm{mc}}\right] \tag{67}$$

with q_{sp} in g cm^{-1} s^{-1}, yielding a correlation coefficient R^2 of 0.880.

In all 33 runs, Eq. (67) correctly predicted suspended load transport when the latter occurred and vice versa. U^* was calculated from the velocity profile, after first straightening out the latter and then adapting the value of U^* until the observed and theoretical velocity profiles Eqs. (21)–(24) coincided as closely as possible.

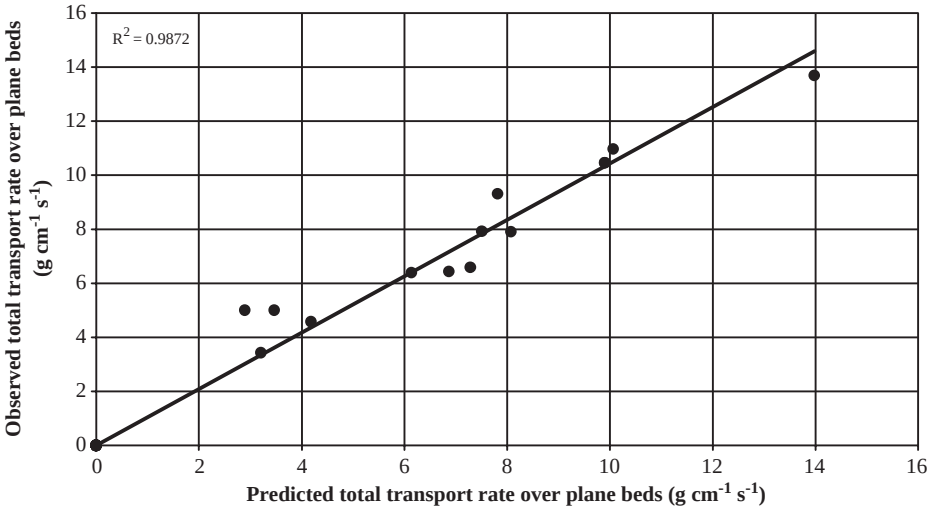

Fig. 18. Plot of total observed sediment discharge over plane beds against the total sediment discharge predicted by Eq. (68), based upon the experiments of Guy et al. (1966).

6.3. Total sediment discharge

The predicted total sediment discharge is given by

$$q_{tp} = q_{bp} + q_{sp}. \quad (68)$$

Fig. 18 plots the predicted total sediment discharge against the observed total discharge over plane beds. The correlation coefficient R^2 in this case is 0.9805. For those runs where q_{bp} excessively overpredicted the observed bedload discharge q_{bo}, the total discharge proves to be less anomalous, indicating that part of the suspended load may have been transported as bedload where and/or when the measurements were taken. Guy et al. (1966) did not consider the saltation load separately and probably incorporated it into the suspension load, which might explain this observation.

7. Application to field conditions

The equations above are in all cases based on laboratory (flume or wind tunnel) data. To determine their validity under natural conditions however, is not always easy, as many published field studies do not provide all the necessary information. This may be because certain parameters are difficult to measure under these circumstances, or because many researchers simply do not state how their information was obtained. For example, water or air temperatures are often not recorded or grain sizes are mentioned without indicating whether they were determined by sieve or settling tube analysis. Velocity profile data are also very seldom provided.

7.1. Field measurement of sediment discharge

A serious problem in sediment transport studies under field conditions, especially in the marine realm, is the accurate measurement of sediment discharge. Sediment traps, for example, disturb the layer in which transport takes place and are selective in the sizes they capture (Dyer, 1976). They also have to be oriented exactly parallel to the transport direction, which is not always known (Pickrill, 1986). Fluorescent tracers need to reach equilibrium with the background, which can take up to about 2 months (Lees, 1983) and during which they may be transported in different directions by tidal currents, waves and storm processes. For these reasons, a method commonly employed by engineers to determine bedload discharge in the marine environment is based on the migration rate of bedforms such as ripples or dunes (e.g., Bagnold, 1941; Kachel and Sternberg, 1971; Langhorne, 1981; Yang, 1986). The bedload discharge (q_{br}) in this case is given by

$$q_{br} = \rho_\gamma H U_r \quad (69)$$

where U_r is the bedform migration rate.

To test whether this approach is feasible, the small-ripple laboratory data of Guy et al. (1966) were examined. Plotting q_{br} against q_{bo} shows that q_{br} generally (but not always) overestimates q_{br} and has a correlation coefficient R^2 of only 0.3963. Plotting q_{br} against the total load ($q_{bo}+q_{so}$) also yields an R^2 value of -0.1902, so that this method appears to be completely unreliable. It is no wonder, therefore, that large discrepancies are commonly observed between predicted and "observed" bedload transport under natural conditions. Heathershaw (1981), for example, tested five of the most frequently used bedload equations on one data set and obtained a two-order magnitude spread in predictions. Different researchers have also found that different equations fit their own particular data best (e.g. Heathershaw and Hammond, 1980; Lees, 1983; Pickrill, 1986).

7.2. Transport equations based on velocities recorded at fixed distances above the bed: are they valid?

An extensive survey of the literature shows that a widespread practice to predict sediment transport rates is to record the current velocity at a fixed distance from the sediment surface, usually between 100 and 200 cm (e.g., O'Brien and Rindlaub, 1936; Miller et al., 1977; Berben et al., 1978; Bórówka, 1980; Black and Healy, 1982; Lees, 1983; Hardisty, 1983; Pickrill, 1986; Yang, 1986; Sarre, 1988; Wang and Gao, 2001). In some cases, equations are used to calculate this velocity from the mean current velocity. Wang and Gao (2001), for example, used the continuity equation ($U_m = Q/dw$) to determine the mean current velocity (Guy et al., 1966) and subsequently obtained U_{100} from

$$U_{100} = U_m - (U^*/K)\ln(0.37d). \quad (70)$$

However, as pointed out by Le Roux (2004a,b,c,d,e), this method gives errors of up to 45% for U_{100} for the well-constrained laboratory data of Guy et al. (1966). Conversely, it means that if U^* were to be calculated from Eq. (70) after measuring the current velocity at 100 cm, it would provide widely erroneous results.

The logarithmic relationship

$$U_y = U^*[2.5\ln(y/y_0)] \quad (71)$$

is also commonly employed to describe wind profiles (e.g., Howard et al., 1978; Namikas, 2003). This equation is in fact the same as Eq. (23), because $y_0 = D \exp(-8.5/2.5)$, or $D/30$ for closely packed, uniform sand-grain roughness. However, for poorly sorted sediments or in the presence of bedforms, the roughness height y_0 changes (Middleton and Southard, 1984). This suggests that y_0 has to be determined for each specific case. In the absence of such data, however, some investigators have used a constant value for y_0. For example, Sarre (1988), in his study of wind transport on a beach in North Devon, England, could not determine a conclusive value for y_0 and therefore used a constant of 0.3 cm (following Bagnold, 1941) for k to estimate y_0 from the equation

$$y_0 = k\exp(-KU_k/U^*) \quad (72)$$

where U_k is the wind speed at height k at the threshold of grain movement (312 cm s^{-1}). The calculated y_0 of 0.0005 cm was subsequently employed in Eq. (71) to determine shear velocities from the wind speed measured at a height of 200 cm. Similarly, Namikas (2003) used a fixed roughness length of $2D_{50}/30$ to model aeolian mass flux on a sandy beach.

To demonstrate that this procedure cannot produce reliable results, consider the case study reported by Svasek and Terwindt (1974) on wind transport along a beach near Noorwijkerhout, the Netherlands. These authors measured velocity profiles and determined the values of U^* using Eq. (25), and y_0 by extrapolating the velocity distribution line in the graph to the ordinate $U=0$, as also described in Section 3.2.4 above. Their Fig. 3 shows two velocity profiles measured under different wind conditions, which have a cross-over point at a height of about 20 cm. For the two profiles, respectively, widely different shear velocities were calculated (48 and 141 cm s^{-1}) and transport rates were measured at 0.1389 and 3.1389 g cm^{-1} s^{-1}. If, instead of measuring complete velocity profiles, they had simply measured the velocity at a height of 100 cm above the surface and used a constant for y_0 of 0.00083 cm for their mean grain size of 0.025 cm, the calculated shear velocities would have been 33 and 47 cm s^{-1}, respectively, very different from the actual values. Furthermore, if the wind speed had been measured at 20 cm, these values would have been exactly the same, obviously not agreeing with the widely different sediment transport rates. It should be noted also that both velocity profiles of Svasek and Terwindt (1974) are described by Eq. (71), in spite of the fact that the Re^* number corresponding to their first profile ($k=0.03$ cm, $\rho=0.0012$ g cm^{-3}, $\mu=0.00018$ g cm^{-1} s^{-1}, $U^*=48$ cm s^{-1}) is only 9.6, which corresponds to transitional flow. It thus appears that wind profiles do not follow the velocity distribution laws given by Eqs. (21)–(23), and that Eq. (71) should not be applied with a constant value of $k=0.3$ cm as proposed by Bagnold (1941) and Sarre (1988).

To further investigate the feasibility of using U_{100} for transport equations, the flume data of Guy et al. (1966) were analyzed for runs over plane beds. U_{100} was determined from the upward projection of the best-fit trendlines to the velocity profile data, after adjusting the profiles slightly up or down to get the highest correlation coefficient (Middleton and Southard, 1984). The velocity 100 cm from the bottom at the threshold of sediment movement (U_{100c}) was calculated from the critical shear velocity for the particular grain size, first converting their settling diameter to the equivalent sieve diameter Eqs. (1),(29) (30) (31) (32) (33),(4) (5) (6) (7),(34) (35) (36) (37) (38), and then using Eqs. (29)–(33) to determine the dimensionless sieve settling diameter and Eqs. (46)–(48) to calculate the dimensionless shear stress β_c. U_c^* was obtained from β_c using Eq. (44) and inserted into the appropriate of Eqs. (21)–(23) to calculate U_{100c}, after determining the Re_c^* number at threshold from Eq. (18), using $k=D_v$ and $U^*=U_c^*$. The ratio U_{100}/U_{100c} was subsequently plotted against the observed bedload discharge for each run (setting $U_{100}/U_{100c}=0$ where $U_{100}<U_{100c}$) to determine its suit-

ability for bedload equations. Fig. 19 shows that this relationship is extremely poor, giving an R^2 of only 0.4417, compared to 0.9066 for U^*_{calc}/U^*_c (Le Roux and Brodalka, 2004).

The considerations above strongly suggest that the use of U_{100} (or any other specific height above the bed), should be abandoned in sediment transport studies, even where it had been determined from velocity profiles. An exception is where U_y can be related to the water depth, for example to determine U_m (at $0.37d$) in Eqs. (21)–(24).

For aeolian transport, where it is impossible to determine the "mean" wind speed in the absence of d, formulas such as Eq. (65) cannot be used. However, it may be possible to substitute U^* and U^*_c for U_m and U_{mc}, respectively, using a different constant for C. The two velocity profiles given by Svasek and Terwindt (1974) suggest that C may have a value of around 2400, but much more data would be required to establish such a relationship. It is clear, however, that complete velocity profiles should be measured instead of relying on single measurements at specific heights above the bed.

Considering the fact that bedload discharge as measured under field conditions using present technology is probably highly inaccurate, and that the velocity profiles required for the application of Eqs. (64)–(68) are not provided in the vast majority of studies, it was not possible to test these equations against field data.

7.3. Threshold of sediment motion by wind

The application of Eqs. (49) and (50) to natural conditions is hampered by the fact that the former were derived only from dry, well sorted grains entrained on flat beds in a wind tunnel. Natural sediments are not necessarily well sorted and smaller grains will be entrained before the D_{50} size. Eqs. (49) and (50) should therefore be considered to yield the maximum shear velocity required to entrain sediment with a median size D_{50}.

Wind tunnel experiments on sand with a D_{50} size of 0.04 cm by Belly (1964), showed that the critical shear velocity at a moisture content of 0.1% vol. water is 35 cm s^{-1}. Using Eqs.)(1),(29)(30)(31)(32)(33), (49),(50) and (44) ($\rho = 0.0012$ g cm^{-3}; $\mu = 0.00018$ g cm^{-1} s^{-1}) for this grain size gives a U^*_c value of 34.4 cm s^{-1}. It thus seems as if a very slight moisture content prevents the finer fraction from being entrained too easily and compensates for the lower expected critical shear velocity of less well sorted sand.

Svasek and Terwindt (1974) studied aeolian transport on a beach with a median size of 0.025 cm. Using velocity profiles, they calculated the mean critical shear velocity for dry, cohesionless sand at 17 cm s^{-1}, which is lower than the 25.7 cm s^{-1} calculated from the equations above, but in line with what is expected for a less well sorted sand. However, for the same sand with a moisture content of 0.1% vol. water,

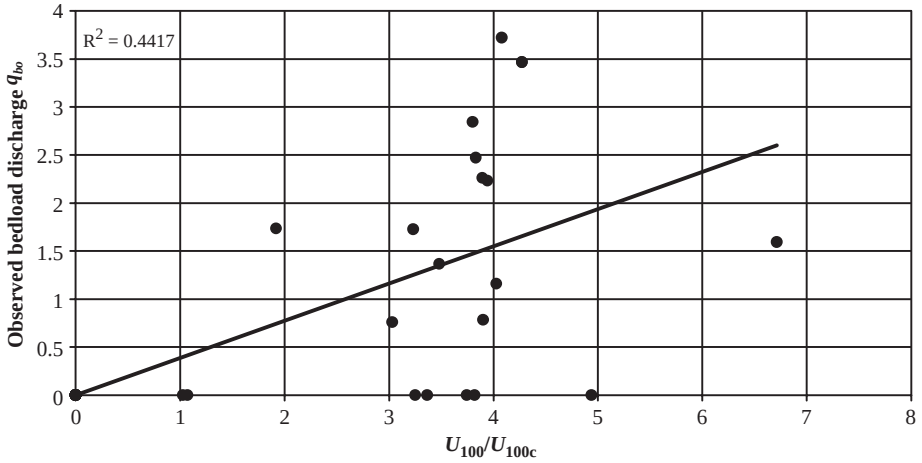

Fig. 19. Plot of U_{100}/U_{100c} ratio against observed bedload discharge over plane beds, based upon the experimental results of Guy et al. (1966).

they obtained U_c^* values of 25.2 and 25.8 cm s^{-1}, respectively (their Fig. 4), which supports the observation above. It is therefore tentatively suggested that Eqs. (49) and (50) may be used directly for natural sands with a moisture content close to about 0.1% vol. water.

7.4. Threshold of sediment motion under waves

Davies (1985) carried out two field experiments during 1978 and 1980, respectively, outside the breaker zone in Start Bay, Devon, in a water depth of 4–10 m. He used synchronous video and near-bed velocity measurements to establish the critical conditions of sediment transport. In contrast to the laboratory studies discussed above, the sediment was poorly sorted and wave conditions were irregular, which was exacerbated by the presence of ripples on the sea bed. However, the latter problem was overcome using a procedure developed earlier (Davies, 1979, 1982).

In the two experiments, Davies (1985) determined the incipient sediment motion, which corresponded to the D_{50} size fraction, as well as the general bedload motion corresponding to the D_{90} size fraction. Table 3 shows the grain-size data and wave periods together with the critical velocities reported by Davies (1985). Unfortunately, Davies (1985) did not report the water temperature, so that a temperature of 15 °C is assumed here. This corresponds to a density of 1.026 g cm^{-3} and a dynamic viscosity of 0.012 g cm^{-1} s^{-1}, assuming a salinity of 35 g kg^{-1}. The critical orbital velocities under these conditions as calculated by the methods of Manohar (1955), Komar and Miller (1975b), and Eqs. (1),(29) (30) (31) (32) (33),(55) and (56) are shown in Table 3. The results indicate an excellent agreement, with the latter equations giving the best overall performance of the three methods.

8. Conclusions

The widespread practice of basing sediment transport equations on single measurements of current velocities at a specific distance above the bed should be abandoned, as it cannot give reliable results. Similarly, fixed roughness lengths should not be used, but must be determined from measured velocity profiles for every specific case. The need for an improved method to determine sediment transport rates under natural conditions is great, as existing techniques are probably highly inaccurate. In particular, the use of bedform migration rates to calculate the bedload discharge appears to be unreliable, as it has a very low correlation coefficient with the actual discharge as measured under laboratory conditions.

The settling velocity of grains, being a hydrodynamic measure of grain size, has a wide application in sediment transport studies. As shown above, it yields good results not only for unidirectional currents of water or air, but also for oscillatory waves. This is because it depends on the same important variables (size, density and shape) that govern sediment transport. The use of dimensionless settling velocities (W_d) together with other dimensionless expressions such as the critical shear stress β_c and wave orbital velocity U_{dw}, greatly facilitates these studies and allows the equations to be applied to a wide range of fluids, gases and grain densities.

The methods described above, although yet to be proven under natural conditions because of the problems mentioned above, are practical in that no difficult-to-obtain parameters are needed. Required variables include the fluid temperature (in the case of sea water, the salinity is also needed to calculate the density and dynamic viscosity), the water depth, the wave period, the sediment grain size as determined by

Table 3
Field data of Davies (1985) and comparison of observed critical orbital velocities with calculated critical orbital velocities

T_w	Grain size (cm)	U_{wc} (cm s^{-1}) Manohar (1955)	U_{wc} (cm s^{-1}) Komar and Miller (1975b)	U_{wc} (cm s^{-1}) This paper	U_{wc} (cm s^{-1}) Davies (1985)
10	0.078 (D_{50})	36	33	36	36
10	0.135 (D_{90})	44	42	43	45
6	0.026 (D_{50})	29	18	23	23
6	0.062 (D_{90})	38	28	28	34

either sieve or settling tube analysis, the grain density, complete velocity profiles, and the types of bedforms. The latter can be photographed with underwater cameras in natural rivers or on the sea floor, determined with a sonic depth sounder, or estimated from the flow and sediment characteristics using the diagrams of Southard and Boguchwal (1990). Natural slopes are normally low, but this should be measured and corrected for where possible.

An Excel program used in velocity profile analysis (Le Roux and Brodalka, 2004) integrates many of the equations in this paper to calculate bedload and suspended load discharge in unidirectional currents. Under natural conditions, it is recommended that a series of velocity profiles be measured across the current, together with sediment data, and that these be integrated to determine the total sediment discharge. The program can be obtained from the *Computers and Geosciences* website, or by writing to the author.

Acknowledgements

J.R.L Allen and Keith Crook suggested very useful improvements to this paper, for which I am grateful.

I am deeply indebted to Norman D. Smith and John B. Southard, who taught me fluid mechanics and stimulated my interest in sediment transport 20 years ago. Some of the material in Sections 2 and 3 was condensed from their course notes.

The organisers of the International Workshop PASSED (Burg Flemming and Daniel Hartmann), where the outline of this paper was originally presented, kindly consented to its publication in this volume.

Appendix A

List of symbols

a	Coefficient used in settling equation based on H_r
A	Surface or cross-sectional area in cm^2
b	Coefficient used in settling equation based on H_r
C	Bedform constant
C_d	Dimensionless drag coefficient
d	Flow depth in cm
d_o	Threshold wave orbital diameter in cm
D	Grain diameter in cm
D_d	Dimensionless grain diameter
D_{dn}	Dimensionless nominal grain diameter
D_{ds}	Dimensionless sphere diameter
D_{dv}	Dimensionless grain sieve diameter
D_{dw}	Dimensionless grain fall diameter
D_I	Intermediate orthogonal grain diameter in cm
D_l	Long orthogonal grain diameter in cm
D_m	Short orthogonal grain diameter in cm
D_n	Nominal grain diameter in cm=1.32 D_v
D_s	Sphere diameter in cm
D_{ds}	Dimensionless sphere diameter
D_v	Grain sieve diameter in cm
D_w	Grain fall diameter in cm
D_{50}	Grain size at 50th percentile
D_{90}	Grain size at 90th percentile
DES	Deviation from equivalent sphere
e	Variable
f_{dw}	Dimensionless wave friction factor
F	Force in g cm s^{-2}
F_D	Drag force in g cm s^{-2}
Fr	Froude number
g	Gravity acceleration in cm s^{-2}
H	Bedform height in cm
H_r	Hofmann shape entropy
K	Von Karman constant (0.4)
k	Bottom roughness in cm
L	Length in cm
m	Number of primary dimensions
M	Mass in g
ME	Mean prediction error in percent
n	Number of variables
p_i	Proportion of intermediate orthogonal grain diameter
p_l	Proportion of long orthogonal grain diameter
p_m	Proportion of short orthogonal grain diameter
q_b	Bedload discharge in g cm^{-1} s^{-1}
q_{bo}	Observed bedload discharge in g cm^{-1} s^{-1}
q_{bp}	Predicted bedload discharge in g cm^{-1} s^{-1}
q_{br}	Bedload discharge as predicted by bedform migration rate, in g cm^{-1} s^{-1}
q_{so}	Observed suspended load discharge in g cm^{-1} s^{-1}

q_{sp} Predicted suspended load discharge in $cm^3\ cm^{-1}\ s^{-1}$
q_{to} Observed total sediment discharge in $g\ cm^{-1}\ s^{-1}$
q_{tp} Predicted total sediment discharge in $g\ cm^{-1}\ s^{-1}$
Q Flow discharge in $cm^3\ s^{-1}$
R^2 Correlation coefficient
Re Reynolds number
Re_f Flow Reynolds number
Re_w Settling Reynolds number
Re^* Boundary Reynolds number
Re^*_c Critical boundary Reynolds number
$Re^*_{c\alpha}$ Critical boundary Reynolds number on slope α
S Channel slope
T Time in s
T_w Wave period in s
U Velocity in $cm\ s^{-1}$
U_{av} Time-averaged flow velocity in $cm\ s^{-1}$
U_c Critical flow velocity on horizontal bed in $cm\ s^{-1}$
U_{dw} Dimensionless wave orbital velocity
U_{dwc} Dimensionless critical orbital velocity
U_k Flow velocity at height k at threshold of sediment movement in $cm\ s^{-1}$
U_m Mean flow velocity in $cm\ s^{-1}$
U_{mc} Mean critical flow velocity in $cm\ s^{-1}$
U_r Bedform velocity in $cm\ s^{-1}$
U_w Wave orbital velocity in $cm\ s^{-1}$
U_{wc} Critical wave orbital velocity in $cm\ s^{-1}$
U_y Current velocity at distance y (cm) from bed in $cm\ s^{-1}$
U_{100} Flow velocity 100 cm above bed in $cm\ s^{-1}$
U_{100c} Flow velocity 100 cm above bed at threshold of sediment movement in $cm\ s^{-1}$
U^* Shear or friction velocity in $cm\ s^{-1}$
U^*_c Critical friction velocity in $cm\ s^{-1}$
U^*_{calc} Critical friction velocity as calculated by minimizing difference between theoretical and observed velocity profiles in $cm\ s^{-1}$
$U^*_{c\alpha}$ Critical friction velocity on slope α
$U_{c\alpha}$ Critical flow velocity on slope α
V Volume in cm^{-3}
w Channel width in cm
W Settling velocity in $cm\ s^{-1}$
W_{dn} Dimensionless nominal sieve diameter settling velocity
W_{dp} Dimensionless predicted settling velocity
W_{ds} Dimensionless sphere settling velocity
W_{dvn} Dimensionless settling velocity of nominal sieve diameter grain
W_{dw} Dimensionless measured settling velocity
W_m Measured settling velocity in $cm\ s^{-1}$
W_{vn} Nominal sieve diameter settling velocity in $cm\ s^{-1}$
W_p Predicted settling velocity in $cm\ s^{-1}$
W_s Settling velocity of sphere in $cm\ s^{-1}$
W_v Sieve diameter settling velocity in $cm\ s^{-1}$
X Bedload discharge given by Eq. (65)
y Distance from bottom
y_a Displacement height in cm
y_d Dimensionless distance from bed
y_0 Roughness length in cm
z Exponent used in settling equation based on DES
α Bedslope angle in degrees
β_c Shields critical dimensionless boundary shear stress
$\beta_{c\alpha}$ Shields critical dimensionless boundary shear stress on slope α
β_w Oscillatory Shields critical dimensionless boundary shear stress
δ Small change in variable
∂ Thickness of viscous sublayer in cm
Δ Difference between variables
ϕ Pivot or internal friction angle in degrees
λ Bedform length in cm
μ Dynamic fluid viscosity in $g\ cm^{-1}\ s^{-1}$
π Pi (22/7)
π_x Dimensionless group of variables
ρ_s Grain density in $g\ cm^{-3}$
ρ Fluid density in $g\ cm^{-3}$
ρ_γ Submerged grain density $(\rho_s - \rho)$ in $g\ cm^{-3}$
τ Shear stress
τ_c Critical boundary shear stress in $g\ cm^{-1}\ s^{-2}$
τ_0 Boundary shear stress in $g\ cm^{-1}\ s^{-2}$
τ_{wc} Critical oscillatory bed shear stress
υ Kinematic fluid viscosity

References

Allen, J.R.L., 1982a. Sedimentary Structures: their Character and Physical Basis, vol. 1. Developments in Sedimentology, vol. 30. Elsevier, Amsterdam.

Allen, J.R.L., 1982b. Simple models for the shape and symmetry of tidal sand waves: 1. Statistically-stable equilibrium forms. Marine Geology 48, 31–49.

Aschenbrenner, B.C., 1956. A new method of expressing particle sphericity. Journal of Sedimentary Petrology 26, 15–31.

Ashida, K., Michiue, M., 1973. Studies on bed-load transport rate in open channel flows. International Symposium on River Mechanics, International Association of Hydraulic Researchers, Bangkok, vol. 1, pp. 407–417.

Baba, J., Komar, P.D., 1981a. Settling velocities of irregular grains at low Reynolds numbers. Journal of Sedimentary Petrology 51, 121–128.

Baba, J., Komar, P.D., 1981b. Measurements and analysis of settling velocities of natural sand grains. Journal of Sedimentary Petrology 51, 631–640.

Bagnold, R.A., 1941. The Physics of Blown Sand and Desert Dunes. Methuen and Company, London (263 pp.).

Bagnold, R.A., 1946. Motion of waves in shallow water. Interaction of waves and sand bottoms. Proceedings of the Royal Society, Series A: Mathematical, Physical and Engineering Sciences 187, 1–15.

Bagnold, R.A., 1963. Mechanics of marine sedimentation. In: Hill, M.N. (Ed.), The Sea, vol. 3. Wiley, New York, pp. 507–582.

Bagnold, R.A., 1966. An approach to the sediment transport problem for general physics. Geological Survey Professional Paper, vol. 422-I. Geological Survey, Washington, DC.

Bennett, J.P., 1995. Algorithm for resistance to flow and transport in sand-bed channels. Journal of Hydraulic Engineering 121, 578–590.

Belly, P.Y., 1964. Sand movement by wind. C.E.R.C. Technical Memo 1 (38 pp.).

Berben, F.M.L., Brouwer, M.J.N., Kohsiek, L.H.M., Lemkes, J.C.A., Steyaert, F.H.I.M., 1978. Ribbelvormen, waterbeweging en hun onderlinge samenhang in een getijdengebied (Plaat van Ossenisse, Westerschelde). Geografisch Instituut, Rijksuniversiteit Utrecht.

Black, K.P., Healy, T.R., 1982. Sediment transport investigations in a New Zealand tidal inlet. Proc. 18th Coastal Engineering Conf., Cape Town. , pp. 2436–2457.

Bórówka, R.K., 1980. Present day processes and dune morphology on the Leba Barrier, Polish coast of the Baltic. Geografiska Annaler 62A, 75–82.

Bridge, J.S., Bennett, S.J., 1992. A model for the entrainment and transport of sediment grains of mixed sizes, shapes, and densities. Water Resources Research 28, 337–363.

Buckingham, E., 1914. On physically similar systems; illustrations of the use of dimensional equations. Physical Review, 2nd series 4, 345–376.

Buckingham, E., 1921. Notes on the methods of dimensions. London Philosophical Magazine, 6th series 42, 696–719.

Buffington, J.M., Montgomery, D.R., 1997. A systematic analysis of eight decades of incipient motion studies, with special reference to gravel-bedded rivers. Water Resources Research 33, 1993–2029.

Chang, H.H., 1988. Fluvial Processes in River Engineering. Wiley, New York.

Cheng, N.S., 1997. Simplified settling velocity formula for sediment particle. Journal of Hydraulic Engineering 123, 149–152.

Chepil, W.S., 1959. Equilibrium of soil grains at the threshold of movement by wind. Proceedings of the Soil Society of America 23, 422–428.

Collins, M.B., Rigler, J.K., 1982. The use of settling velocity in defining the initiation of motion of heavy mineral grains, under unidirectional flow. Sedimentology 29, 419–426.

Corey, A.T., 1949. Influence of Shape on the Fall Velocity of Sand Grains. Unpubl. M.Sc. Thesis, A and M College, Colorado, 102 pp.

Davies, A.G., 1979. The potential flow over ripples on the seabed. Journal of Marine Research 37, 743–759.

Davies, A.G., 1982. On the interaction between surface waves and undulations on the seabed. Journal of Marine Research 40, 331–368.

Davies, A.G., 1985. Field observations of the threshold of sediment motion by wave action. Sedimentology 32, 685–704.

Dietrich, W.E., 1982. Settling velocity of natural particles. Water Resources Research 18, 1615–1626.

Dobkins, J.E., Folk, R.L., 1970. Shape development on Taiti-Nui. Journal of Sedimentary Petrology 40, 1167–1203.

Dyer, K.R, 1976. The measurement of bed shear stresses and bedload transport rates. In: Wiley, M. (Ed.), Estuarine Processes, vol. 7. Academic Press, New York, pp. 124–135.

Dyer, K.R., 1986. Coastal and Estuarine Sediment Dynamics. Wiley, Chichester. 342 pp.

Engelund, F., Fredsoe, J., 1976. Transition from dunes to plane bed in alluvial channels. Institute of Hydrodynamic and Hydraulic Engineering, Technical University of Denmark, Series Paper 4.

Everts, C.H., 1973. Particle overpassing on flat granular boundaries. Proceedings of the American Society of Civil Engineering 99, 425–438.

Ferguson, R.I., Church, M., 2004. A simple equation for grain settling velocity. Journal of Sedimentary Research 74, 933–937.

Gibbs, R.J., Matthews, M.D., Link, D.A., 1971. The relationship between sphere size and settling velocity. Journal of Sedimentary Petrology 41, 7–18.

Govers, G., 1987. Initiation of motion in overland flow. Sedimentology 34, 1157–1164.

Graf, W.H., 1971. Hydraulics of Sediment Transport. McGraw-Hill Book Co., New York, N.Y. 513 pp.

Guy, H.P., Simons, D.B., Richardson, E.V., 1966. Summary of alluvial channel data from flume experiments 1955–1961. U.S. Geological Survey Professional Paper 462-I (92 p.).

Hallermeier, R.J., 1981. Terminal settling velocity of commonly occurring sand grains. Sedimentology 28, 859–865.

Hammond, T.M., Collins, M.B., 1979. On the threshold of transport of sand-sized sediment under the combined influence of unidirectional and oscillatory flow. Sedimentology 26, 795–812.

Hardisty, J., 1983. An assessment and calibration of formulations for Bagnold's bedload equation. Journal of Sedimentary Petrology 53, 1007–1010.

Heathershaw, A.D., 1981. Comparison of measured and predicted transport rates in tidal currents. Marine Geology 42, 75–104.

Heathershaw, A.D., Hammond, F.D.C., 1980. Transport and deposition of non-cohesive sediments in Swansea Bay. In: Collins, M.B., Banner, F.T., Tyler, P.A., Wakefield, S.J., Jones, A.E. (Eds.), Industrialised Embayments and their Environmental Problems, a Case Study of Swansea Bay. Pergamon Press, Oxford. 616 pp.

Hjulstrom, F., 1935. Studies in the morphological activity of rivers as illustrated by the River Fyris. Geological Institute, University of Uppsala. Bulletin 25, 221–528.

Hjulstrom, F., 1939. Transportation of detritus by moving water. In: Trask, P.D. (Ed.), Recent Marine Sediments, a Symposium, Society of Economic Paleontologists Mineralogists, Spec. Publ., vol. 4, pp. 5–31.

Hofmann, H.J., 1994. Grain-shape indices and isometric graphs. Journal of Sedimentary Research A64, 916–920.

Howard, A.D., Morton, J.B., Gad-El-Hak, M., Pierce, D.B., 1978. Sand transport model of barchan dune equilibrium. Sedimentology 25, 307–338.

Inman, D.L., 1949. Sorting of sediments in the light of fluid mechanics. Journal of Sedimentary Petrology 19, 51–70.

Illenberger, W.K., 1991. Pebble shape (and size!). Journal of Sedimentary Petrology 61, 756–767.

Iversen, J.D., White, B.R., 1982. Saltation threshold on Earth, Mars and Venus. Sedimentology 29, 111–119.

Janke, N.C., 1965. Empirical formula for velocities and Reynolds numbers of single settling spheres. Journal of Sedimentary Petrology 35, 749–750.

Janke, N.C., 1966. Effect of shape upon settling velocity of regular convex geometric particles. Journal of Sedimentary Petrology 36, 370–376.

Kachel, N.B., Sternberg, R.W., 1971. Transport of bed load as ripples during an ebb current. Marine Geology 10, 229–244.

Kench, P.S., McLean, R.F., 1997. A comparison of settling and sieve techniques for the analysis of bioclastic sediments. Sedimentary Geology 109, 111–119.

Komar, P.D., 1980. Settling velocity of circular cylinders at low Reynolds numbers. Journal of Geology 88, 327–336.

Komar, P.D., Clemens, K.E., 1985. The relationship between a grain's settling velocity and threshold of motion under unidirectional currents. Journal of Sedimentary Petrology 56, 258–266.

Komar, P.D., Cui, B., 1984. The analysis of grain-size measurements by sieving and settling-tube techniques. Journal of Sedimentary Petrology 54, 603–614.

Komar, P.D., Miller, M.C., 1973. Sediment threshold under oscillatory water waves. Journal of Sedimentary Petrology 43, 1101–1110.

Komar, P.D., Miller, M.C., 1975a. On the comparison between the threshold of sediment motion under waves and unidirectional currents with a discussion on the practical evaluation of the threshold. Journal of Sedimentary Petrology 45, 362–367.

Komar, P.D., Miller, M.C., 1975b. Sediment threshold under oscillatory waves. Proc. 14th Int. Conf. Coastal Engineering, 1974. American Society of Civil Engineers, pp. 756–775.

Komar, P.D., Reimers, C.E., 1978. Grain shape effects on settling rates. Journal of Geology 86, 193–209.

Krumbein, W.C., 1941. Measurement and geological significance of shape and roundness of sedimentary particles. Journal of Sedimentary Petrology 11, 64–72.

Lane, E., 1955. Design of stable channels. Transactions of the American Society of Civil Engineers 120, 1260–12344.

Langhorne, D.N., 1981. An evaluation of Bagnold's dimensionless coefficient of proportionality using measurements of sandwave movement. Marine Geology 43, 49–64.

Lees, B.J., 1983. The relationship of sediment transport rates and paths to sandbanks in a tidally dominated area off the coast of East Anglia, U.K.. Sedimentology 30, 461–485.

Le Roux, J.P., 1990. Flume study on the concentration of ilmenite in fine-grained sand and implications concerning uranium mineralisation in the Beaufort Group. South African Journal of Geology 93, 785–794.

Le Roux, J.P., 1991a. Flume experiments on permeability and organic matter as related to the genesis of stratiform uranium deposits in the Beaufort Group. South African Journal of Geology 94, 212–219.

Le Roux, J.P., 1991b. A rapid method to determine the critical shear stress for sphere entrainment under unidirectional fluid flow. Sedimentary Geology 75, 1–3.

Le Roux, J.P., 1992a. Settling velocity of spheres: a new approach. Sedimentary Geology 81, 11–16.

Le Roux, J.P., 1992b. Behavior of spherical grains in fluids: a convenient spreadsheet template for engineers and sedimentologists. Computers & Geosciences 18, 1255–1257.

Le Roux, J.P., 1993. Genesis of stratiform U–Mo deposits in the Karoo Basin of South Africa. Ore Geology Reviews 7, 485–509.

Le Roux, J.P., 1996. Settling velocity of ellipsoidal grains as related to shape entropy. Sedimentary Geology 101, 15–20.

Le Roux, J.P., 1997a. Comparison of sphericity indices as related to the hydraulic equivalence of settling grains. Journal of Sedimentary Research 67, 527–530.

Le Roux, J.P., 1997b. Relationship between aerodynamic entrainment threshold and hydrodynamic settling velocity of particles. Sedimentary Geology 109, 199–205.

Le Roux, J.P., 1997c. An Excel program for computing the dynamic properties of particles in Newtonian fluids. Computers & Geosciences 23, 671–675.

Le Roux, J.P., 1998. Entrainment threshold of natural grains in liquids determined empirically from dimensionless settling velocities and other measures of grain-size. Sedimentary Geology 119, 17–23.

Le Roux, J.P., 2001a. Threshold of particle transport under oscillatory waves. Proceedings 7th International Conference of the International Association of Mathematical Geology, Cancun (on CD).

Le Roux, J.P., 2001b. A simple method to predict the threshold of particle transport under oscillatory waves. Sedimentary Geology 143, 59–70.

Le Roux, J.P., 2002a. Application of the Hofmann shape entropy to determine the settling velocity of irregular, semi-ellipsoidal grains. Sedimentary Geology 149, 237–243.

Le Roux, J.P., 2002b. Shape entropy and settling velocity of natural grains. Journal of Sedimentary Research 72, 363–366.

Le Roux, J.P., 2002c. Aerodynamic and geometric diameter of airborne particles—discussion. Journal of Sedimentary Research 72, 441–442.

Le Roux, J.P., 2002d. Wave friction factor as related to the Shields parameter for steady currents. Sedimentary Geology 155, 37–43.

Le Roux, J.P., 2004a. A simple method to predict the threshold of particle transport under oscillatory waves, by J.P. Le Roux, Sedimentary Geology 143 (2001), 59–70—reply to discussion. Sedimentary Geology 163, 327–330.

Le Roux, J.P., 2004b. A hydrodynamic classification of grain shapes. Journal of Sedimentary Research 74, 135–143.

Le Roux, J.P., 2004c. An integrated law of the wall for hydrodynamically transitional flow over plane beds. Sedimentary Geology 163, 311–321.

Le Roux, J.P., 2004d. Particle Size, Shape, Settling Velocity and Transport. Abstracts PASSED: International Sedimentological Workshop. Hanse Institute for Advanced Studies, Delmenhorst.

Le Roux, J.P., 2004e. Erratum to "Discussion of: Le Roux, J.P. (2001). A simple method to predict the threshold of particle transport under oscillatory waves" [Sediment. Geol. 143 (2001) 59–70: reply to discussion. Sedimentary Geology, 167, 109.

Le Roux, J.P., 2005. Determination of drag coefficients in measuring particle diameters—discussion. Journal of Sedimentary Research 75, 520–523.

Le Roux, J.P., Brodalka, M., 2004. An Excel-VBA program for the analysis of current velocity profiles. Computers & Geosciences 30, 867–879.

Le Roux, J.P., Brynard, H.J., 1994. A strategy for uranium exploration in the Permo-Triassic Beaufort Group of the main Karoo Basin, South Africa. Journal of African Earth Sciences 18, 245–253.

Luque, R.F., Van Beek, R., 1976. Erosion and transport of bed-load sediments. Journal of Hydraulic Research 14, 127–144.

Madsen, O.S., Grant, W.D., 1975. The threshold of sediment movement under oscillatory waves: a discussion. Journal of Sedimentary Petrology 45, 360–362.

Manohar, M., 1955. Mechanics of bottom sediment movement due to wave action. Beach Erosion Board. Technical Memo 75.

McNown, J.S., Malaika, J., 1950. Effect of particle shape on settling velocity at low Reynolds numbers. American Geophysical Union Transactions 31, 74–82.

Meyer-Peter, E., Muller, R., 1948. Formulas for Bed-Load Transport, Second Meeting. International Association of Hydraulic Researchers, Stockholm.

Middleton, G.V., Southard, J.B., 1984. Mechanics of sediment movement, 2nd ed. Lecture Notes for Short Course, vol. 3. Society of Economic Paleontologists and Mineralogists, Rhode Island. 400 pp.

Miller, M.C., Komar, P.D., 1977. The development of sediment threshold curves for unusual environments (Mars) and for inadequately studied materials (foram sands). Sedimentology 24, 709–721.

Miller, M.C., McCave, I.N., Komar, P.D., 1977. Threshold of sediment motion under unidirectional currents. Sedimentology 24, 507–527.

Namikas, S.L., 2003. Field measurement and numeric modelling of aeolian mass flux distributions on a sandy beach. Sedimentology 50, 303–326.

Nickling, W.G., 1988. The initiation of particle movement by wind. Sedimentology 35, 499–511.

Niño, Y., Lopez, F., Garcia, M., 2003. Threshold for particle entrainment into suspension. Sedimentology 50, 247–264.

O'Brien, M.P., Rindlaub, B.D., 1936. The transport of sand by wind. Civil Engineering 6, 325–327.

Paintal, A.S., 1971. A stochastic model for bed load transport. Journal of Hydraulic Research 9, 527–553.

Paola, C., 1983. Flow and Skin Friction over Natural Rough Beds, Massachusetts Institute of Technology, Department of Earth and Planetary Sciences, Ph.D. Thesis, 347 pp.

Pettijohn, F.J., 1975. Sedimentary Rocks, 3rd edition. Harper and Row, New York, N.Y. 628 pp.

Pickrill, R.A., 1986. Sediment pathways and transport rates through a tide-dominated entrance, Rangaunu Harbor, New Zealand. Sedimentology 33, 887–898.

Rance, P.J., Warren, N.F., 1969. The threshold of movement of coarse material in oscillatory flow. Proceedings of the 11th Coastal Engineering Conference. ASCE, New York, pp. 487–491.

Reynolds, O., 1883. An experimental investigation of the circumstances which determine whether the motion of water shall be direct or simuous, and the law of resistance in parallel channels. Philosophical Transactions of the Royal Society of London 174, 935–982.

Rigler, J.K., Collins, M.B., 1983. Initial grain motion under oscillatory flow: a comparison of some threshold criteria. Geo-Marine Letters 3, 43–48.

Rouse, H., 1936. Nomogram for the settling velocity of spheres. National Research Council Committee on Sedimentation Publication, 57–64.

Rubey, W., 1933. Settling velocities of gravel, sand and silt particles. American Journal of Science 25, 325–338.

Sarre, R.D., 1988. Evaluation of aeolian sand transport equations using intertidal zone measurements, Saunton Sands, England. Sedimentology 35, 671–679.

Shields, A., 1936. Anwendung der Ahnlichkeits Mechanik und der Turbulenzforschung auf die Geschiebe Bewegung, vol. 26. Mitteilungen Preuss. Versuchanstalt für Wasserbau and Schiffbau, Berlin. 26 pp.

Sleath, J.F.A., 1977. Sediment transport by waves. Report CUED/A-Hydraulics/TR1. Engineering Department, Cambridge University, Cambridge, England.

Sneed, E.D., Folk, R.L., 1958. Pebbles in the lower Colorado River, Texas—a study in particle morphogenesis. Journal of Geology 66, 114–150.

Soulsby, R.L., Whitehouse, R.J.S., 1997. Threshold of sediment motion in coastal environments. Pacific Coasts and Ports '97, 13th Australasian Coastal and Engineering Conference and 6th Australasian Port and Harbour Conference, 1997, Christchurch, New Zealand. HR Wallingford, Oxon, pp. 149–154.

Southard, J.B., Boguchwal, L.A., 1990. Bed configurations in depth–velocity size diagrams. Journal of Sedimentary Petrology 41, 903–915.

Stokes, G.G., 1851. On the effect of the internal friction on the motion of pendulums. Cambridge Philosophical Transactions 9, 8–106.

Stringham, G.E., Simons, D.B., Guy, H.P., 1969. The behavior of large particles falling in quiescent liquids. Geological Survey of America Professional Paper 562-c (36 pp.).

Sundborg, A., 1956. The River Klaälven: a study in fluvial processes. Geografiska Annaler, Stockholm 38, 125–316.

Svasek, J.N., Terwindt, J.H.J., 1974. Measurement of sand transport by wind on a natural beach. Sedimentology 21, 311–322.

Vanoni, V.A., 1964. Measurements of Critical Shear Stress for Entraining Fine Sediments in a Boundary Layer. California Institute of Technology, W.M. Keck Laboratory of Hydraulics and Water Resources, Report KH-R-7. 47 pp.

Van Rijn, L.C., 1984. Sediment transport: Part II. Suspended load transport. Journal of Hydraulic Engineering 110, 1613–1641.

Van Rijn, L.C., 1993. Principles of Sediment Transport in Rivers, Estuaries and Coastal Seas. Aqua Publications, Amsterdam.

Wadell, H., 1932. Volume, shape and roundness of rock particles. Journal of Geology 40, 443–451.

Wadell, H., 1933. Sphericity and roundness of rock particles. Journal of Geology 41, 310–331.

Wang, Y.P., Gao, S., 2001. Modification to the Hardisty equation, regarding the relationship between sediment transport rate and particle size. Journal of Sedimentary Research 71, 118–121.

Warg, J.B., 1973. An analysis of methods for calculating constant terminal-settling velocities of spheres in liquids. Mathematical Geology 5, 59–72.

Wentworth, C.K., 1922. The shapes of beach pebbles. U.S. Geological Survey, Professional Paper 131-C, 75–83.

Whitehouse, R.J.S., Hardisty, J., 1988. Experimental assessment of two theories for the effect of bedslope on the threshold of bedload transport. Marine Geology 79, 135–139.

Wiberg, P.L., Smith, J.D., 1987. Calculations of the critical shear stress for motion of uniform and heterogeneous sediments. Water Resources Research 23, 1471–1480.

Wilcock, P.R., 1993. Critical shear stress of natural sediments. Journal of Hydraulic Engineering 119, 491–505.

Willetts, B.B., Rice, M.A., Swaine, S.E., 1982. Shape effects in aeolian grain transport. Sedimentology 29, 409–417.

Williams, G.P., 1966. Particle roundness and surface texture effects on fall velocity. Journal of Sedimentary Petrology 36, 255–259.

Williams, J.J., Butterfield, G.R., Clark, D.G., 1994. Aerodynamic entrainment threshold: effects of boundary layer flow conditions. Sedimentology 41, 309–328.

Winkelmolen, A.M., 1982. Critical remarks on grain parameters, with special emphasis on shape. Sedimentology 29, 255–265.

Yalin, M.S., 1977. Mechanics of Sediment Transport. Pergamon Press, New York, N.Y. 298 pp.

Yalin, M.S., Karahan, E., 1979. Inception of sediment transport. Proceedings of the American Society of Civil Engineering. Journal of the Hydraulics Division 105, 1433–1443.

Yang, C., 1986. On Bagnold's sediment transport equation in tidal marine environments and the practical definition of bedload. Sedimentology 33, 465–486.

You, Z.J., Yin, B.S., 2004. A discussion of the paper "A simple method to predict the threshold of particle transport under oscillatory waves, by J.P. Le Roux, Sedimentary Geology 143 (2001), 59–70". Sedimentary Geology 163, 323–325.

Zhu, L.J., Cheng, N.S., 1993. Settling of sediment particles. Research Report, Department of River and Harbor Engineering-Nanjing Hydraulic Research Institute, Nanjing. (in Chinese).

Zingg, A.W., 1953. Some characteristics of aeolian sand movement by saltation process. Editions Centre National Recherche Scientifique 13, 197–203.